A Comparative Study of the Frequency Ratio, Analytical Hierarchy Process, Artificial Neural Networks and Fuzzy Logic Methods for Landslide Susceptibility Mapping: Taşkent (Konya), Turkey

Adnan Ozdemir

Abstract In this study, the four landslide susceptibility (LS) mapping methods, frequency ratio (FR), analytic hierarchy process (AHP), artificial neural networks (ANN) and fuzzy logic (FL) method, are compared. The study has been conducted in Taşkent (Konya, Turkey) Basin which is located between 36.88 N to 36.95 N latitudes and 32.35 E to 32.53 E longitudes. The survey area is approximately 80 km^2. The FR, AHP, ANN and FL methods are used to map LS. Thematic layers of fourteen landslide conditioning factors including landslide inventory, elevation, slope, slope aspect, plan, and profile curvature, sediment loading factor, stream power, and wetness index, drainage, and fault density, distance to drainage, and fault, geological units, and land use-land cover are used for preparing the LS maps. Estimation power of models has been evaluated by the relative operating characteristic curve method. The areas under the curve for FR, AHP, ANN and FL method have been computed as 0.926, 0.899, 0.916 and 0.842, respectively. These results showed that FR method is relatively good, whereas FL method is a relatively poor estimator for susceptibility. The validity of the LS maps was evaluated by test landslides. The 58 test landslides (76 pixels), 43 training landslides (200 pixels), and 101 total landslides (276 pixels) have been put onto the LS maps prepared by the various methods. The percentages of the existing landslide pixels within the different landslide occurrence potential classes were determined. It is determined that a significant portion of all landslides (76% in the ANN, 83% in the FR, 87% in the AHP and 89% in the FL method) belong to the high and very high LS class. The produced four susceptibility maps were also compared using cross-correlation methods. The cross-correlation coefficients were found to be 0.82, 0.70, 0.63, 0.54, 0.48, and 0.45 for AHP versus FR, FR versus FL, AHP versus FL, AHP versus ANN, FR versus ANN, and FL versus ANN maps, respectively. Here, the confidence level is 0.95. The FR and AHP methods have been assessed to be more suitable methods among other used methods.

1 Introduction

Landslides cause a lot of loss of life in the world. At the same time, landslides are damaging the environment. In some countries, landslides can cause more lives and property losses than earthquakes, and floods (García-Rodríguez et al. 2008). Therefore, it is very important to identify landslide sensitive areas and to

A. Ozdemir (✉)
Department of Civil Engineering, Necmettin Erbakan University, Konya, Turkey
e-mail: aozdemir3@hotmail.com

make LS maps (Mohammady et al. 2010). Landslide susceptibility (LS) mapping provide information to the relevant executive administrations to locate the landslide susceptible areas and make decisions about preventive plans (Mahdavifar 1997). Particularly in the last two decades, numerous methods have been developed and applied in LS studies. In recent years, LS methods combined with GIS have been used more frequently. These methods are summarized by Guzzetti et al. (1999). In this study, FR, AHP, ANN and FL methods have been used and compared for LS mapping in Taşkent (Konya, Turkey) Basin.

There have been many studies using the frequency ratios (FR) (Akgun et al. 2008; Dahal et al. 2008; Van Westen et al. 2008; Vijith and Madhu 2008; Oh et al. 2009; Ozdemir 2009; Pirasteh et al. 2009; Youssef et al. 2009; Pradhan and Youssef 2010; Regmi et al.2010; Yilmaz 2010; and Ozdemir and Altural 2013) and AHP method (Barredo et al. 2000; Mwasi 2001; Nie et al. 2001; Yagi 2003; Gorsevski et al. 2006; Yalcin 2008; Intarawichian and Dasananda 2010) in LS studies The fuzzy set based methods (Kanungo et al. 2008; Muthu et al. 2008; Pradhan et al. 2009; Pradhan 2010a, b), and ANNs methods (Melchiorre et al. 2006, 2008; Chen et al.2009; Pradhan et al. 2009; Pradhan and Lee 2010a, b; Poudyal et al. 2010; Pradhan and Pirasteh 2010; Pradhan and Buchroithner 2010; Pradhan et al. 2010a, b; Yilmaz 2010) have been implemented for landslide susceptibility zone (LSZ) studies. Although there are many methods in use on the mapping of landslide susceptibility, there is no consensus on the best method yet.

There are also many scientific studies on the comparison of LS methods (e.g., Suzen and Doyuran 2004; Ayalew et al. 2005; Brenning 2005; Yesilnacar and Topal 2005; Kanungo et al. 2006; Lee 2007; Meisina and Scarabelli 2007; Yalcin 2008; Magliuloü et al. 2009; Rossi et al. 2009; Yilmaz 2009; Miner et al. 2010; Poudyal et al. 2010; Pradhan and Lee 2010b, c; Van Den Eeckhaut et al. 2010; Yilmaz 2010; Akgun 2012; Pradhan 2011; Yalcin et al. 2011; Mohammady et al. 2012; Teimouri and Graee 2012; Zhu and Wang 2009; Ozdemir and Altural 2013;). For example, a comparative study of WOE, AHP, ANN, and Generalized Linear Regression procedures for LS mapping is presented by the Vahidnia et al. (2009). Kanungo et al. (2006) compared ANN, fuzzy combined neural and fuzzy weighting procedures. Lee (2005a, b), Lee and Sambath (2006), Lee and Pradhan (2007) and Oh

et al. (2009) compared logistic regression with a FR approach and found out that logistic regression was generally more accurate. Pradhan and Lee (2010a) compared ANNs with FR and regression method. Similarly, Yilmaz (2010) compared ANNs with conditional probability, logistic regression and support vector machine and found logistic regression to be the most accurate. Nefeslioglu et al. (2008) compared logistic regression with an artificial neural network (ANN) and found that while the ANN has over-predicted the susceptibility whereas the logistic regression model has under-predicted. Paulin and Bursik (2009) combined the logistic regression model with an ANN in a GIS framework. Suzen and Doyuran (2003) made a comparison of bivariate and multivariate methods in the same study area.

The main objectives of the study are: (1) to prepare LS maps of Taşkent Basin; (2) to evaluate, compare and verify some LS mapping methods. In this study, AHP, FR, ANN and FL methods were studied and the results were compared; (3) to determine the best methods for evaluating the LS in the research area, and (4) to assess and map the LS areas based on the best method of the considered methods.

2 Study Area

The research area is located approximately between latitudes from 18° 06′ 00″ N to 18° 38′ 24″ N and longitudes from 98° 04′ 12″ E to 98° 38′ 24″ E, covering an area of about 80 km^2 in the vicinity of Taşkent, Konya (Fig. 1).

Based on the meteorological data of 22 years in the vicinity of Taşkent region, In the region, the coldest month is February with an average of 6.7 °C and the hottest is August with 23.2 °C. The annual average temperature of the study area is 17.9 °C. According to precipitation measurements between 1975 and 2015, it was determined that precipitation height ranged between 587 and 700 mm. The annual average precipitation of Taşkent town is 838 mm. Precipitation usually falls in winter as snow and rain. In the Taşkent basin, the topographic altitude ranges from 1063 m to 2111 m. Slope angles range from 0° to 63° (average angle 19°). In the northern part of the Taşkent basin, the aspect of the slope is in general to the north and in the southern part of the basin to the north. Dominant vegetation includes grapes and mixed
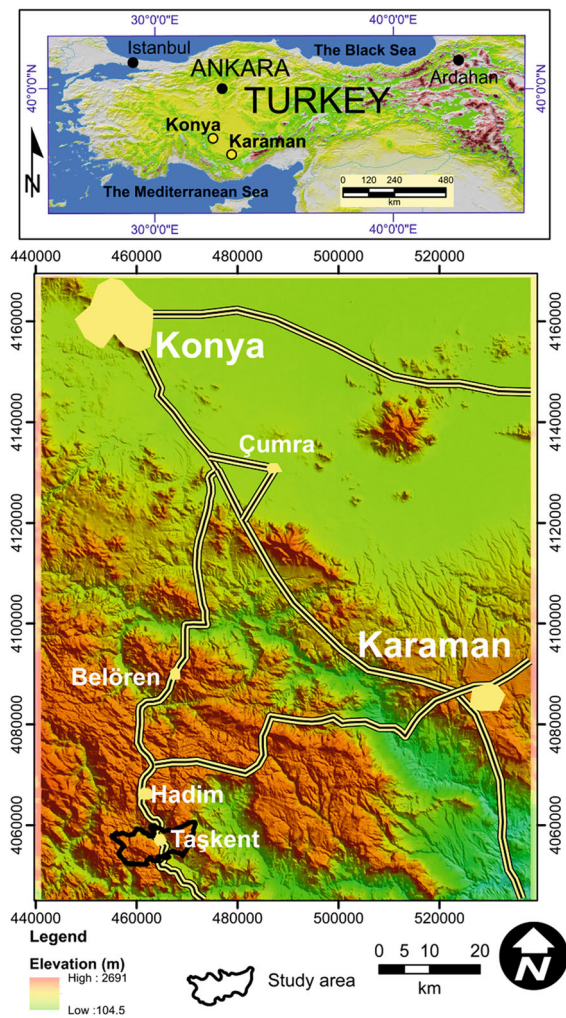
Fig. 1 Location map of study area

deciduous trees below 1500 m, a mixed pine forest from 1500 to 2000 m alternating with the hills, and an evergreen forest that extends up to 2100 m.

3 Materials and Methodology

The methodology used in this study includes seven steps: (1) Preparation of landslide inventory map of the study area from field surveys; (2) Identification of conditioning factors and the use of GIS to produce the landslide conditioning factor maps; (3) Application of various methods (FR, NN, FL and AHP) for the mapping of LS; (5) Use of GIS to produce the LS maps; (6) Testing reliability of the LS maps produced

in a location of Taşkent (Konya-Turkey) vicinity and; (7) Comparison of results obtained from the LS maps.

In the following section, information about the landslide inventory map, used in the investigation, and the factors affecting the landslide formation, are given.

3.1 Preparation of Landslide Inventory Map

There was no landslide inventory map of the study area. Landslide scars areas were mapped by field studies. A total of 101 landslide areas (Table 1, Fig. 2) and 37 non-landslide areas were mapped and used in this study. Landslides combined cover an area of 72913 m^2, accounting for 0.09% of the total study area. The minimum, mean and maximum landslide areas are 18 m^2, 904 m^2 and 20419 m^2, respectively. The polygonal areas of landslides and non-landslides were converted into points using GIS software. This resulted in 377 points (276 points for landslides and 101 points for non-landslides). 76 random numbers were generated between 1 and 276, and the landslide point numbers corresponding to these generated numbers were used as the test landslides. Similarly, 38 random numbers were generated between 1 and 101, and the non-landslide point numbers corresponding to these generated numbers were used as the test non-landslide points (Table 2). In other word, the landslide and non-landslides points were randomly sampled from the inventory. In the FR, AHP and FL methods, 276 landslide points (200 for analysis and 76 for testing) have been used. In the ANN method, 263 points (200 landslide and 63 non-landslide points) for training and 114 points (76 landslide and 38 non-landslide points) for testing have been used.

3.2 Selected Landslide Conditioning Factors Used in the Susceptibility Mapping

The causes of landslides are directly or indirectly related to slope angle, slope aspect, stream power index, topographic wetness index, sediment loading factor, geology, distance from drainage system, distance from lineament, and land use (Poudyal et al. 2010). In this study, 14 factors which are considered to be effective in landslide formation were selected and used. These are elevation, slope gradient, slope aspect, plan curvature, profile curvature, sediment loading capacity index, stream power index, wetness index, drainage density, distance to the drainage, geology,

Table 1 Coordinates of landslide points in the study area

ID	Area (m²)	X	Y	ID	Area (m²)	X	Y
1	4354	455,669	408,6280	51	1230	456,762	408,7710
2	452	455,019	408,641,0	52	782	456,875	408,764,0
3	558	455,088	408,640,0	53	985	456,787	408,791,0
4	104	455,419	408,645,0	54	718	456,921	408,788,0
5	657	455,471	408,648,0	55	1254	457,313	408,755,0
6	834	455,538	408,652,0	56	806	457,364	408,760,0
7	283	455,579	408,654,0	57	599	457,387	408,767,0
8	411	455,626	4086540	58	1028	457425	408,775,0
9	947	455,660	408,657,0	59	574	457,120	408,809,0
10	20419	455,751	408,671,0	60	5142	457,320	408,807,0
11	740	455,653	408,687,0	61	2402	457,349	408,849,0
12	1623	455,715	4086900	62	922	457,645	408,839,0
13	341	455,789	408,690,0	63	7652	457,844	408,848,0
14	1783	455,882	408,688,0	64	1608	457,604	4088610
15	698	455,545	408,678,0	65	561	457,636	408,878,0
16	173	455,571	4086710	66	680	457,922	408,868,0
17	182	455,562	408,673,0	67	762	457,983	408,875,0
18	73	455,588	408,673,0	68	547	458,001	4088820
19	54	455,597	408,674,0	69	461	455,120	408,508,0
20	52	455,578	408,674,0	70	120	454,875	408,489,0
21	54	455,614	4086730	71	53	454,826	408,459,0
22	108	455,597	408,671,0	72	190	454,640	408,452,0
23	149	455,623	408,671,0	73	258	454,580	408,363,0
24	52	455,640	4086720	74	153	453,147	408,390,0
25	45	455,655	408,671,0	75	269	453,283	408,547,0
26	54	455,645	408,674,0	76	103	453,420	408,475,0
27	42	455,628	408,674,0	77	45	454,962	408,686,0
28	18	455,556	408,675,0	78	35	454,245	408,714,0
29	38	455,593	408,676,0	79	72	451,737	408,809,0
30	40	455,610	408,676,0	80	120	450,351	408,777,0
31	52	455,631	408,678,0	81	24	450393	408,783,0
32	60	455,624	408,677,0	82	36	452,905	408,764,0
33	139	455,644	408,677,0	83	79	452,865	408,765,0
34	98	455632	408,675,0	84	94	451,906	4087830
35	27	455,618	408,674,0	85	39	451,878	408,794,0
36	137	455,585	408,679,0	86	81	451,850	408,796,0
37	89	455,605	408,680,0	87	67	457,197	4087490
38	160	455,624	408,681,0	88	111	455,622	408,474,0
39	1496	455,830	408,701,0	89	172	455,553	408,427,0
40	929	455,947	4086980	90	28	456,466	408,381,0
41	1185	456,042	408,706,0	91	50	456,182	408,374,0
42	1660	455,973	408,711,0	92	133	456,433	408,378,0
43	1628	456,140	408,721,0	93	515	446,740	408,613,0
44	1999	456,239	408,712,0	94	40	446,399	408,612,0
45	1211	456,376	408,732,0	95	55	453,988	4087210

Table 1 continued

ID	Area (m^2)	X	Y	ID	Area (m^2)	X	Y
46	956	456,624	408,737,0	96	88	453,528	408,749,0
47	824	456,678	4087500	97	71	453,483	4087560
48	648	456,722	408,759,0	98	115	453,476	408,760,0
49	704	456,631	408,766,0	99	158	452,806	408,499,0
50	9622	456,592	408,783,0	100	212	452,104	408,425,0
				101	50	451,905	408,441,0
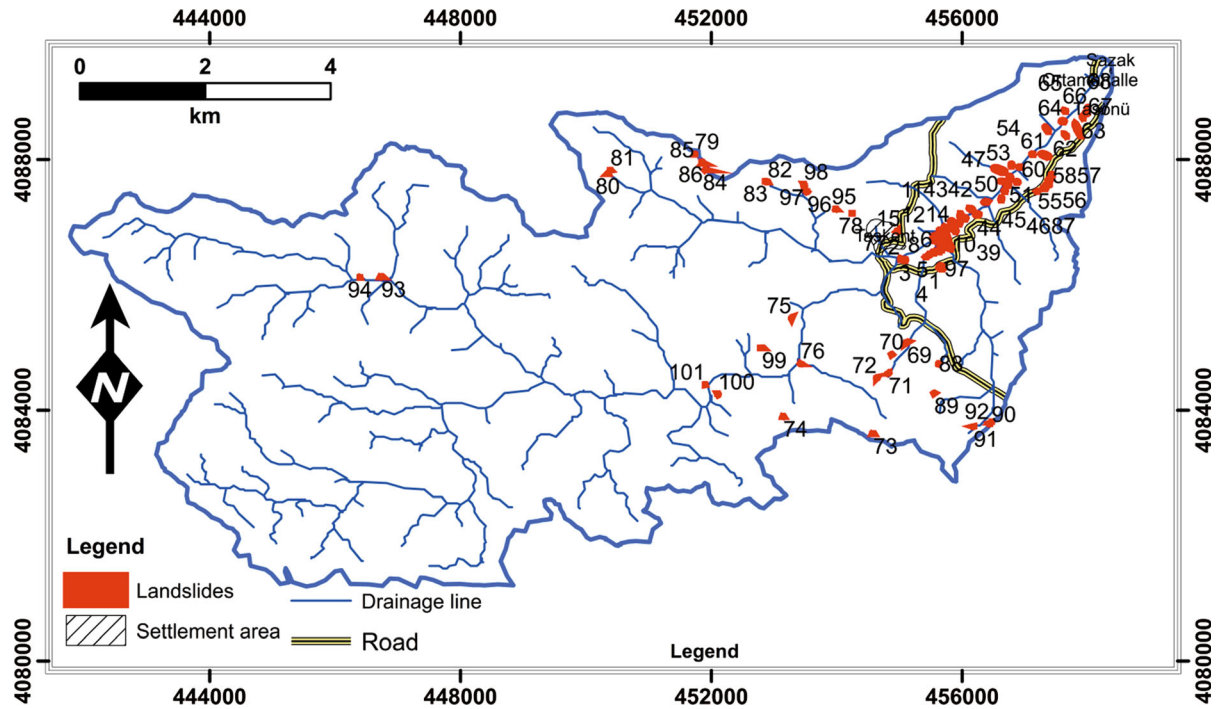
Fig. 2 Landslide inventory map

fault density, distance to the fault and land use/land cover. Some of the landslide conditioning factors were derived from the geology map. The geology and land use maps are prepared by digitizing the hard copy maps manually.

3.2.1 DEM and Its Derivatives

The DEM was prepared by digitizing topographic maps of the area. Some landslide conditioning factors, such as elevation, slope aspect, slope angle, plan, and profile curvature, sediment loading factor, wetness index and stream power index were derived from the DEM.

3.2.1.1 Elevation Due to the fact that precipitation, freezing and thawing phenomena are higher, more landslides can occur in high altitude areas (Menendez Duarte and Marqinez 2002; Lin and Tung 2003). However, due to the presence of more durable lithologies in high altitude terrain, sometimes fewer landslides can also occur in these areas. (Dai and Lee 2002; Zhou et al. 2002; Cevik and Topal 2003; Ayalew et al. 2004; Lan et al. 2004). Some researchers have suggested that topographic height has little contribution to the formation of landslides (Guzzetti et al. 1999; Lineback Gritzner et al. 2001; Ayalew and Yamagishi 2005). However, in the investigated area, there are higher strength lithologies in the high land

sections. The range of elevation is from 1063 to 1961 m, gradually increasing from North-East to South-West (Fig. 3a). Landslides below 1508 m are dominant (94%) for lithology of the geological units that have clay compositions.

3.2.1.2 Slope   The slope angle is the main factor in the formation of landslides (Lee and Min 2001; Fernandez et al. 2008; Mousavi 2017). The high slope angle produces a high shear force, which makes it easier to slip (Jones et al. 1961). Therefore, slope angle is considered as a factor controlling the formation of the landslide in the susceptibility studies (Dai et al. 2001a, b; Cevik and Topal 2003; Lee 2005a; Yalcin 2008; Nefeslioglu et al. 2008). The slope angle map was prepared for angles ranging from 0° to 63° (Fig. 3b).

3.2.1.3 Slope Aspect   Some authors reported that the slope aspect is the important factors in preparing LS maps (Guzzetti et al. 1999; Nagarajan et al. 2000; Saha et al. 2002; Cevik and Topal 2003; Lee et al. 2004; Lee 2005a). In the northern hemisphere, the north-facing slopes have less sunshine, and as a result, these slopes can be colder. On these slopes, snow can melt more slowly and as a result of this, the infiltration of water into the soil may be more (Mousavi 2017). For these reasons, the slope aspect is considered as an effective factor in the formation of landslides (Clerici et al. 2006). In this study, the slope aspect map of the investigated area was produced and used for LS analysis (Fig. 3c).

3.2.1.4 Plan and Profile Curvature   Ercanoglu and Gokceoglu (2002) defined that "the term curvature is generally defined as the curvature of a line formed by

Fig. 3 Some factor maps that affect landslide formation: ▶ **a** elevation; **b** slope; **c** slope aspect; **d** plan curvature; **e** profile curvature; **f** sediment loading factor; **g** stream power index, **h** wetness index; **i** drainage density and **j** distance to drainage

the intersection of a random plane with the terrain surface. A value of positive, negative and zero curvature indicate that the surface is upwardly convex, concave and flat at that pixel, respectively. In this study, plan and profile curvature raster maps, produced from DEM were classified in two classes as positive and negative curvature areas (Fig. 3d, e). In the Taşkent Basin, it was determined that the landslides occur more in negative curvature areas.

3.2.1.5 Sediment Transport Capacity (STI), Stream Power Index (SPI), and Topographical Wetness Index (TWI)   These indices are hydrological based terrain indices. Detailed information about these indices is given in Wilson and Gallant (2000) and Saaty and Vargas (2001). Details about the use of these indices in susceptibility maps are given by Pradhan (2010a, b, c), Yilmaz (2010) and Gritzner et al. (2001).

The STI index is used to express the erosion power of surface runoff water. This index gives information about the degree of soil erosion. The values of STI are found to vary between 0 and 232 and STI map is classified into five classes (Fig. 3f). SPI gives information about the eroding power of flowing water from the stream (Moore et al. 1993). The values of SPI are found to vary between 0 and 23420 and SPI map is also classified into five classes (Fig. 3g). TWI provides information on where more surface water can be collected (Nefeslioglu et al. 2008).

Table 2 Polygone and point landslide numbers and its percent in this study used

	Polygone numbers	Polygone numbers (%)	Point (cell) numbers	Point (cell) numbers (%)
Training landslides (A)	43	42.5	200	72.5
Test landslides (T)	58	57.5	76	27.5
Total landslides	101	100	276	100
Training nonlandslides (AN)	22	38.6	63	62.4
Test nonlandslides (TN)	15	40.5	38	37.6
Total non-landslides	37	100	101	100
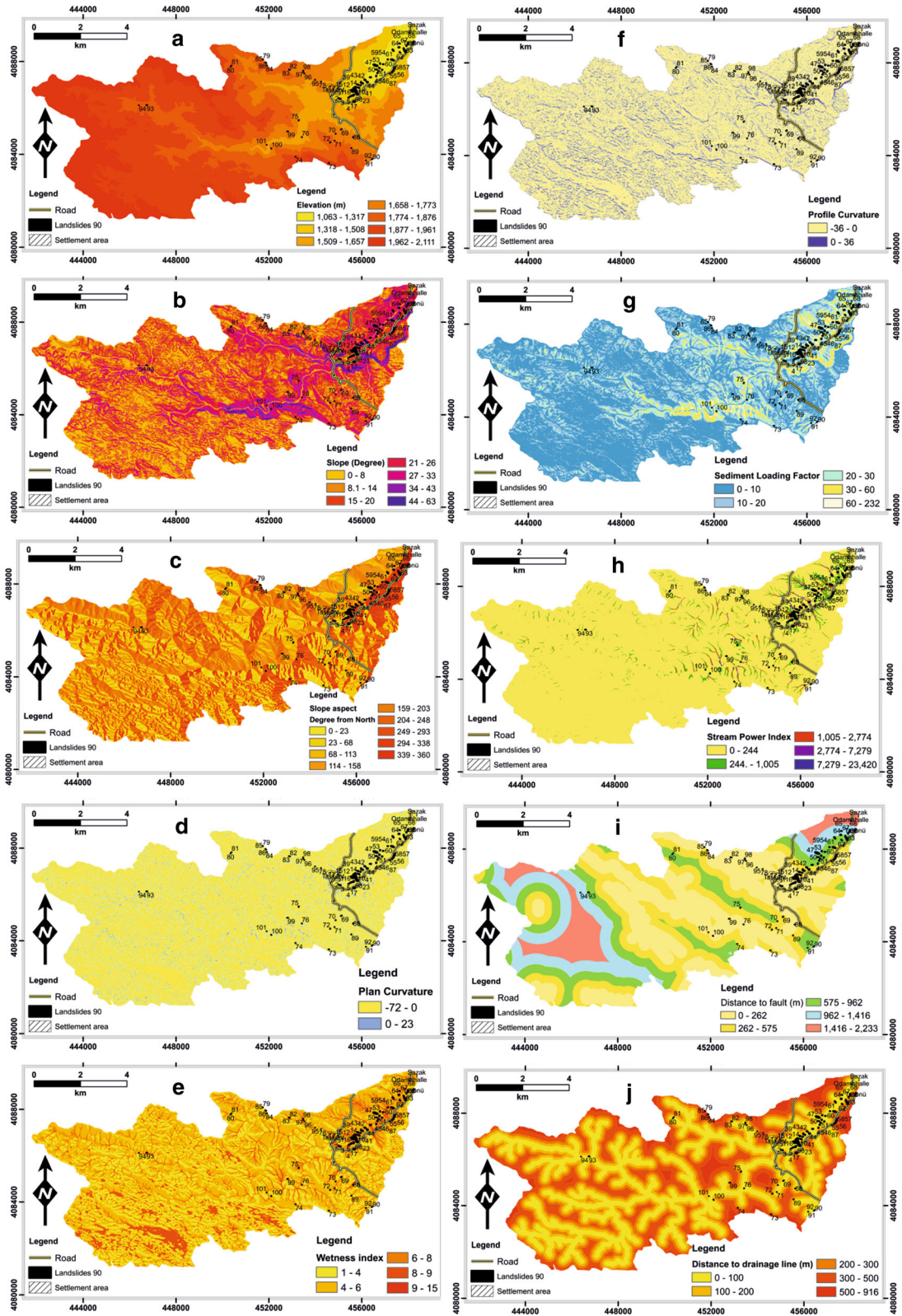
3.2.2 Proximity Maps (Distance to Drainage and Distance to Faults)

Two proximity-based factors evaluated in this study: distance to drainage lines and faults. As you approach the drainage lines, the water content of the slope material increases, and even becomes saturated with water. Again, as the drainage lines approach, the erosion increases in the slope toe. For these reasons, drainage lines may adversely affect slope stability (Gokceoglu and Gokceoglu 1996; Dai et al. 2001a; Saha et al. 2002). The drainage lines used in the study were extracted with GIS software (Tarboton 2003). In the investigated area, the distance to the drainage lines varies between 0 and 916 m (Fig. 3j). The discontinuity of the slope material increases in the areas close to the faults. The more discontinuities in the slope material, the easier the slope will slide (Van Westen and Bonilla 1990; Pachauri and Pant 1992; Luzi and Pergalani 1999; Uromeihy and Mahdavifar 2000; Saha et al. 2002). On the other hand, fault density and distance to faults affect the seismicity of the region. Especially in area with active faults or in area close to active faults, landslides may occur depending on the triggering of earthquakes (Mousavi et al. 2011; Mousavi et al. 2018). For this reason, seismicity of the region can also be evaluated as a factor in slope susceptibility studies especially in tectonically active regions. However, the study area is located in the region of lower seismicity in Turkey. Therefore, seismicity was not considered as a factor in this study. The faults have been drawn from the geological map. In the map of proximity to the faults, the distance values were found to be between 0 and 2233 m (Fig. 4b).

3.2.3 Density Maps (Fault and Drainage Density Maps)

Density maps, such as fault and drainage density maps, are a major parameter in LS analysis. They are generally used in producing LS maps (Pachauri et al. 1998, and Nagarajan et al. 2000). Drainage density was considered as an influential parameter (Suzen and Doyuran 2004; Melchiorre et al. 2010) in this study. Drainage lines are extracted from the DEM. The drainage density map was produced by calculating the cumulative lengths of stream segments of the drainage

Fig. 4 Some factor maps that affect the landslide formation: ▶ **a** fault density; **b** distance to fault; **c** land use and d geological map

network falling within unit areas of 1 km2. They are grouped into five classes (Figs. 3i, 4a).
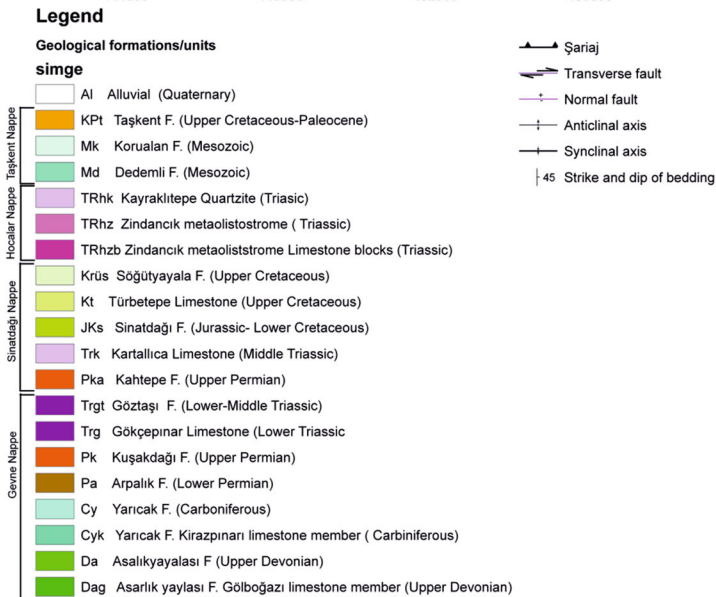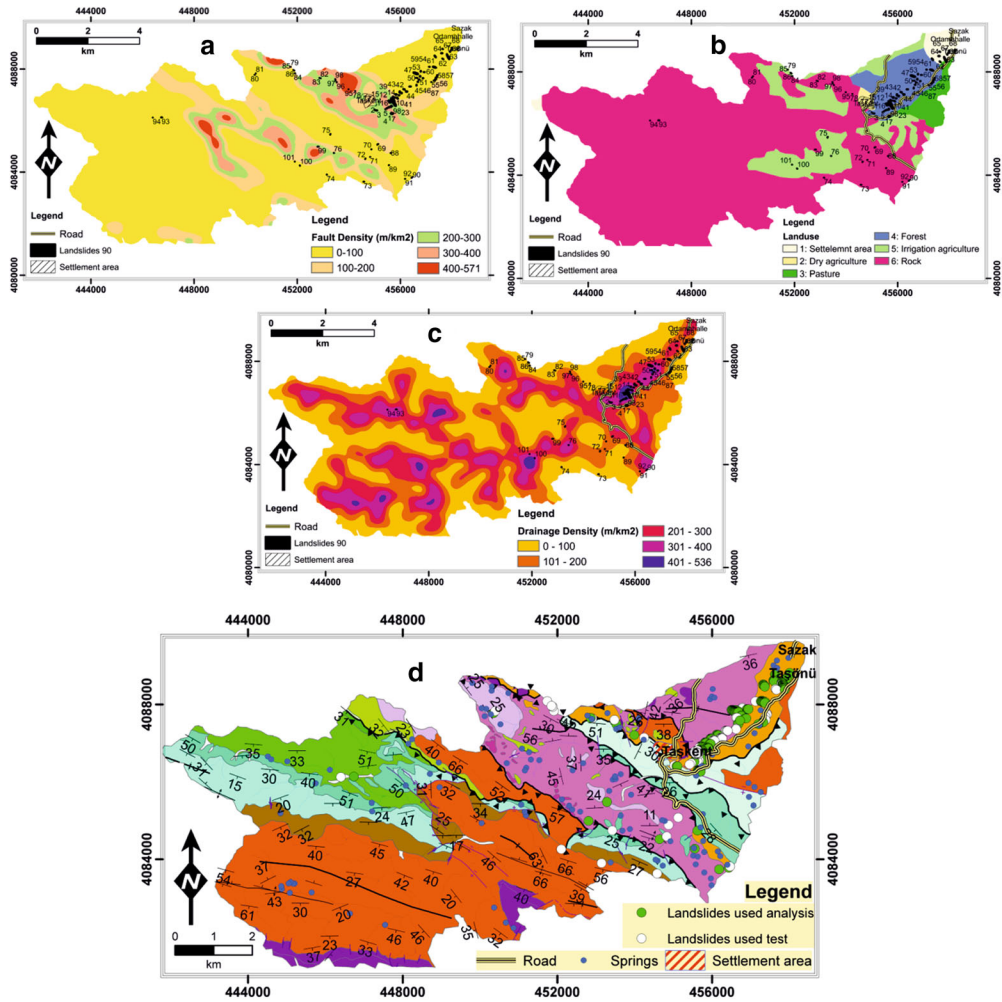
3.2.4 Land Use Map

Land use is the most commonly used human-induced factor on the slope instability (Tangestani 2004; Begueria 2006). This map is generally used in producing LS maps. This map provides information about the land cover. Again, this map provides important information about the purpose of the land use. Several researchers (Jakob 2000; Tangestani 2004; Begueria 2006; Bathurst et al. 2010) have revealed a clear relationship between vegetation cover and slope stability, especially for shallow landslides. Slopes lacking vegetation are more unstable than forest areas (Anbalgan 1992; Turrini and Visintainer 1998; Cannon 2000; Nagarajan et al. 2000; Dai et al. 2001a; Glade 2003).Land cover and land use are thought to be an effective factor in landslide formation. Therefore, this factor was chosen and evaluated in this study on LS. This map was prepared using Land Use (wealth, richness) map of Konya Province. The land use map is classified as follows: "residential area", "forest", "rocky land", "pasture land", "irrigated agriculture land", and "dry agriculture land" (Fig. 4c).

3.2.5 Geology of the Study Area

Lithology and structure are very important in the formation of landslides. Many researchers have used geology and structure as a factor in LS analysis (Anbalgan 1992; Pachauri et al. 1998; Dai et al. 2001a; van Westen et al. 2003; Ayalew and Yamagishi 2005; Ayenew and Barbieri 2005; Ermini et al. 2005; Lee and Talib 2005).

Distribution of the geological units-formations is given in Fig. 4d. In the Tashkent region, the age of the rocks varies between Upper Devonian and Quaternary. The investigated region geologically consists of volcanic, metamorphic and sedimentary rocks. The detailed study of the geology of the Taşkent basin has been given by Turan (1990).

Legend

Geological formations/units

simge

	Al	Alluvial (Quaternary)
Taşkent Nappe	KPt	Taşkent F. (Upper Cretaceous-Paleocene)
	Mk	Korualan F. (Mesozoic)
	Md	Dedemli F. (Mesozoic)
Hocalar Nappe	TRhk	Kayraklıtepe Quartzite (Triasic)
	TRhz	Zindancık metaolistostrome (Triassic)
	TRhzb	Zindancık metaolististrome Limestone blocks (Triassic)
Sinatdağı Nappe	Krüs	Söğütyayala F. (Upper Cretaceous)
	Kt	Türbetepe Limestone (Upper Cretaceous)
	JKs	Sinatdağı F. (Jurassic- Lower Cretaceous)
	Trk	Kartallıca Limestone (Middle Triassic)
	Pka	Kahtepe F. (Upper Permian)
Gevne Nappe	Trgt	Göztaşı F. (Lower-Middle Triassic)
	Trg	Gökçepınar Limestone (Lower Triassic
	Pk	Kuşakdağı F. (Upper Permian)
	Pa	Arpalık F. (Lower Permian)
	Cy	Yarıcak F. (Carboniferous)
	Cyk	Yarıcak F. Kirazpınarı limestone member (Carbiniferous)
	Da	Asalıkyayalası F (Upper Devonian)
	Dag	Asarlık yaylası F. Gölboğazı limestone member (Upper Devonian)

Şariaj

Transverse fault

Normal fault

Anticlinal axis

Synclinal axis

45 Strike and dip of bedding

Bedrock in the region is represented by rocks of Gevne Group (Upper Devonian to Lower –Middle Triassic sedimentary rocks), Sinatdağı Group (Upper Permian to Upper Cretaceous), Hocalar Group (Triassic) and Taşkent Group (Mesozoic to Paleocene). These rock sequences are separated by thrust faults. Gevne Group is sub-divided into six formations as Asarlık Yaylası, Yarıcak, Arpalık, Kuşakdağı, Gökçepınar and Göztaşı Formations. The Asarlık yaylası formation (Da) and its member, the Gölboğazı Limestone (Dag), are the oldest units in the study area. The Lately–Devonian aged Asarlık Yaylası formation consists of sedimentary units, such as dolomitized limestone, sandstone with quartzite, grey and black shale and white limestone. The Yarıcak Formation (Cy, Carbiniferous) and its member, Kirazpınarı limestone (Cyk, Carboniferous), conformably overlies to the Asarlık yaylası Formation. The formation consists of grey-black limestone and an alternating sequence of limestone with sandy, sandstone and limestone. This formation is mapped eastern parts of the investigated area. Yarıcak formation is overlain by the Arpalık Formation (Pa). Arpalık Formation (Lower Permian) mainly consists of greenish-yellow medium to thick limestone bedding with fossils, reddish-black yellow sandstone with quartzite. It is conformably overlain by the Kuşakdağı Formation (Upper Permian). Kuşakdağı Formation (Pk) consists of medium to thick, jointed, hard, grey-black limestone beds, sandy shale, sandy limestone and sandstone with quartzite. As can be seen from Fig. 4d, 35% of the total surface of the study area is covered by this formation. Gökçepınar Limestone (Lower Triassic) conformably overlies to the Kuşakdağı Formation. The Gökçepınar Limestone (Trg) is composed of grey and purple limestone beddings. Gökçepınar Limestone is observed in south western part of the study area. This formation is overlain by the Göztaşı Formation (Trgt, Lower-Middle Triassic). Gevne Group is thrusted over the Sinatdağı Group. Sinatdağı Group is sub-divided into five formations as Kahtepe Formation (Upper Permian), Kartallıca Limestone (Triassic), Sinatdağı Formation (Jurassic-Lower Crecacous), Türbetepe Limestone (Upper Cretaceous) and Söğütyayla Formation (Upper Cretaceous). Kahtepe Formation (Pka) consists of dark grey, partly oolitic and dolomitize limestone, shale and sandstone with limestone intercalations. Kartallıca Limestone unconformably overlies the Kahtepe Formation.

Kartallıca Limestone (Trk) is formed of grey, purple crystallized limestone beds. The Sinatdağı formation (Tod) of Jurassic Lower Crecacous unconformably overlies the Kartallıca Limestone and consists of sedimentary units such as reddish sandy and muddy conglomerate, sandstone, siltstone, and mudstone. The Sinatdağı Formation (Jks) starts with a basal conglomerate on an erosional surface of pre-Jurassic rocks and continues upward with an alternation of various lithologies such as sandstone, siltstone, and mudstone. The conglomerates are grey- and yellow in colour. Pebbles are rounded to sub-rounded. At the top, it is overlain unconformably by Türbetepe limestone (Kt). Söğütyayla formation (Krus) starts with detrital sediments, laminated mudstone, conglomerate, sandstone, shale and dark grey clayey mudstone and continues upward with an alternation of mudstone and sandstone beds. At the top, it mainly consists of a flysch matrix and limestone olistolites. Sinatdağı group is thrusted over the Hocalar group. Hocalar Group is sub-divided into two formations as Zindancık meta-olistostrome-limestone blocks (Trhzb, Triassic) and Kayraktepe Quartzite (Trhk). The Triassic meta-olistostrome and limestone rocks mainly consist of a flysch matrix and limestone olistolites. The flysch matrix is also composed of meta-sandstone, phyllite and slate with quartzite, chlorite, marble, sandy mudstone, and recrystallized limestone. Kayraktepe quartzite mainly consists of dark grey, reddish quartzite and siltstones. Hocalar Group is thrusted over the Taşkent Group. Taşkent Group are sub-divided into three formations as Dedemli (Md, Mesozoic), Korualan (Mk, Mesozoic) and Taşkent ofiolitic complex (Kpt, Upper Cretaceous-Paleocene). Dedemli formation is formed of the various rocks such as tuff, tuffite, basic volcanic, limestone, and chert. Hocalar Group is tectonically overlies the Dedemli formation. Korualan formation starts with a medium to thick beds of limestone, clayey limestone intercalations, and continues upward with an alternation of various lithologies such as white dolomite and dolomitic limestone. At the top, it mainly consists of nodular cherty limestones. This formation is thrusted over the Hocalar group. The Taşkent Melange rocks mainly consist of a flysch matrix, serpentine, pyrocsenite, chert and limestone olistolites. The flysch matrix is also composed of sandstone and mudstone intercalations and conglomerate. The Taşkent Melange were folded and fractured. The rocks are

intensively fractured. Quaternary alluvial discordantly overlie the Taşkent Melange rocks (Fig. 4d).

3.3 Susceptibility Mapping Models Used

In this paper, four different methods, FR, FL, AHP, and ANN, were applied to LS mapping analysis and their performances were compared. Details of these applications have been presented below.

3.3.1 Frequency Ratio (FR) Model

Bonham-Carter (1994) and Lee and Pradhan (2007) have been described Frequency Ratio (FR) method as follows "the ratio of relative frequency of landslide cells in a category (N_{Li}/N_L) to the relative frequency of all landslide cells in the area (N_{Ci}/N_C).

$$FR = (N_{Li}/N_L)/(N_{Ci}/N_C) \qquad (1)$$

where N_{Li} is the number of landslide cells in the class i. N_L is total number of landslide cells. N_{Ci} is the total number of cells in the class i. N_C is the total number of cells.

FR values greater than 1 indicate that landslide formation is high. FR values were calculated for each class of each factor (Table 3). Values of the FR were than summed to calculate the LS index (Lee and Pradhan 2007). Produced LS map was given in Fig. 5a.

3.3.2 Analytic Hierarchy Processes (AHP)

The Analytic Hierarchy Process (AHP) is developed by Saaty (1980). Daneshvar and Bagherzadeh (2010) has been determined that "AHP is a multi-objective, multi-criteria decision-making approach to arrive at a scale of preference among a set of alternatives." Yalcin (2008) describes the use of this method as follows: "this method is widely used in site selection, suitability analysis, regional planning, and landslides susceptibility analysis." Factor weights for each criterion are determined by a pairwise comparison matrix as described by Saaty (1990, 1994) and Saaty and Vargas (2001). The detailed information for the application of the AHP for LS mapping was given by Barredo et al. (2000), Mwasi (2001), Nie H et al. (2001), Yagi (2003), Yalcin (2008), Moradi et al. (2012) and Teimouri and Graee (2012).

According to the Voogd (1982) the steps of the method are as follows: "(1) the complex unstructured problem is broken down into its component factors. The 14 landslide conditioning factors were chosen in this study; (2) each factor is classified into sub classes based on their relative influence on landslide; (3) the relative importance of each class of factors is quantitatively determined by pairwise comparison; (4) the weights of each class on each factor are calculated; (5) the weights of all of the factors are calculated; (6) values of the landslide susceptibility index (LSI) for each considered factor is calculated by summing each factor's weight multiplied by the class weight of each referred factor (for that pixel)."

The obtained weights of conditioning factors (Wj) and the ratings (wij) of various classes are also given in Table 3. The LSI map is established according to Eq. 1. In this study, the CR is found to be 0.068, a ratio which indicates a reasonable level of consistency in the pair-wise comparison that was good enough to recognize the factor weights (Intarawichian and Dasananda 2010). For all the cases of the gained class weights, the CRs are less than 0.1, a ratio which indicates a reasonable level of consistency in the pair-wise comparison that was good enough to recognize the class weights (Pourghasemi et al. 2012; Intarawichian and Dasananda 2010).

$$LSI = \sum_{i=1}^{n} (W_i \times R_i) \qquad (2)$$

where LSI is the landslide susceptibility index of a given pixel, Ri and Wi are the class weights. The factor weights are given in Table 3. The produced LS map is given in Fig. 5b.

3.3.3 Artificial Neural Network (ANN) Method and Its Implementation

The multi-layer ANN model is typically composed of three types of layers: input hidden, and output layers. ANN algorithms calculate the weights for the input values and for the layer nodes of input, hidden and output layers by introducing the input in a feed forward manner, which propagates through the hidden layer to the output layer (Pajanowski et al. 2002). The hidden layer gives an "activation function. It transforms the sum of the input data into feature using one of many possible functions, including exponential,

Table 3 Data employed in the analyses and results obtained from the FR [total number cells of study area (N_C = 797104), and total number cells of training landslides (N_{Cl} = 200). FR = (N_{Li}/N_L)/(N_{Ci}/N_{Cl}), and AHP method

Factor	Range of class	Class no	Fr Area of class (km²) (N_{Li})	Cell number of class (N_{Ci})	Landslide cell number in class (N_{Li})	Frequency ratio, FR = [(N_{Li}/N_L)/(N_{Ci}/N_{Cl})]	AHP Class rates	Class weights (R)	General factor rates	General factor weights (W)	Weights (R × W)
Elevation (m)	1063–1317	1	2.8326	28326	142	19.9797	9	0.321	0.1194	8	0.0383274
Total ΣFr = 24.7	1317–1508	2	4.2073	42073	45	4.2628	7	0.25			0.02985
CI = 4,4Exp(−8)	1508–1657	3	7.0431	70431	1	0.0566	2	0.0714			0.00852516
CR = 3,4Exp(−8)	1657–1773	4	10.9592	109592	9	0.3273	5	0.179			0.0213726
Table value = 1.32	1773–1876	5	13.5027	135027	3	0.0885	3	0.107			0.0127758
	1876–1961	6	27.7970	277970	0	0.0000	1	0.0357			0.00426258
	1961–2111	7	13.3685	133685	0	0.0000	1	0.0357			0.00426258
	No data		0.0909	909	0	0.0000					
Slope (°)	0–8	1	13.6886	136886	12	0.3494	3	0.0857	0.0597	4	0.00511629
Σ Fr = 7.5	8_14	2	18.9452	189452	26	0.5470	4	0.1143			0.00682371
CI = 0	14–20	3	21.6141	216141	35	0.6454	5	0.1429			0.00853113
CR = 0	20–26	4	14.7854	147854	67	1.8060	7	0.2			0.01194
Table value = 1.32	26–33	5	7.5412	75412	49	2.5896	9	0.2571			0.01534887
	33–43	6	2.6543	26543	11	1.6517	6	0.1714			0.01023258
	43–63	7	0.4816	4816	0	0.0000	1	0.0286			0.00170742
	No data		0.0909	909	0	0.0000					
Aspect (°)	0–23	1	7.1689	71689	11	0.6115	5	0.1064	0.07463	5	0.00794063
Σ Fr = 9.6	23–68	2	12.8307	128307	13	0.4038	7	0.1489			0.01111241
CI = 0	68–113	3	8.8897	88897	7	0.3138	6	0.1277			0.00953025
CR = 0	113–158	4	10.0263	100263	28	1.1130	1	0.0213			0.00158962
Table value = 1.45	158–203	5	12.7007	127007	30	0.9414	4	0.0851			0.00635101
	203–2485	6	9.6340	96340	1	0.0414	3	0.0638			0.00476139
	248–293	7	5.0991	50991	2	0.1563	9	0.1915			0.01429165
	293–338	8	8.0274	80274	82	4.0712	8	0.1702			0.01270203
	338–360	9	5.3336	53336	26	1.9428	4	0.0851			0.00635101
	No data		0.0909	909	0	0.0000					

Table 3 continued

Factor	Range of class	Class no	Fr				AHP				Weights (R × W)
			Area of class (km²) (N_Li)	Cell number of class (N_Ci)	Landslide cell number in class (N_Li)	Frequency ratio, FR = [(N_Li/N_L)/(N_Ci/N_C)]	Class rates	Class weights (R)	General factor rates	General factor weights (W)	
Plan curvature	_72_0	1	68.8124	688124	189	1.0954	3	0.75	0.014925	1	0.01119375
ΣFr = 1.5	0_23	2	10.9538	109538	11	0.4005	1	0.25			0.00373125
CI = − 0.5	No Data		0.0351	351	0	0.0000					
CR = − 0.86											
Table value = 0.58											
Profil curvature	_36_0	1	68.7347	687347	189	1.0967	3	0.75	0.014925	1	0.01119375
ΣFr = 1.5	0–36	2	11.0315	110315	11	0.3977	1	0.25			0.00373125
CI = − 0.5; CR = − 0.86	No data		0.0351	351	0	0.0000					
Table value = 0.5											
Sediment loading factor	0–10	1	41.3672	413672	13	0.1253	1	0.04	0.08956	6	0.0035824
	10_20	2	23.2334	232334	39	0.6695	3	0.12			0.0107472
ΣFr = 23.2	20–30	3	8.9840	89840	66	2.9300	5	0.2			0.017912
CI = 0	30–60	4	5.5425	55425	74	5.3249	9	0.36			0.0322416
CR = 0	60–232	5	0.6391	6391	8	4.9924	7	0.28			0.0250768
Table value = 1.49	No data		0.0351	351	0	0.0000					
Stream power index	0–244	1	75.6382	756382	138	0.7277	2	0.0833	0.1194	8	0.00994602
	244–1005	2	3.3697	33697	51	6.0363	7	0.2917			0.03482898
ΣFr = 23.2	1005–2774	3	0.5946	5946	7	4.6953	5	0.2083			0.02487102
CI = 0	2774–7279	4	0.1357	1357	4	11.7563	9	0.375			0.044775
CR = 0	7279–23420	5	0.0280	280	0	0.0000	1	0.0417			0.00497898
Table value = 1.49	No Data		0.0351	351	0	0.0000					
Wetness index	1_4	1	25.7964	257964	15	0.2319	1	0.04	0.07463	5	0.0029852
ΣFr = 9.7	4_6	2	38.3515	383515	113	1.1751	5	0.2			0.014926
CI = 0	6_8	3	7.9794	79794	50	2.4991	7	0.28			0.0208964
CR = 0	8_9	4	6.7185	67185	10	0.5936	3	0.12			0.0089556
Table value = 1.49	9_15	5	0.9204	9204	12	5.1999	9	0.36			0.0268668
	No Data		0.0351	351	0	0.0000					

Table 3 continued

Factor	Range of class	Class no	Fr				AHP				Weights (R × W)
			Area of class (km²) (N_Li)	Cell number of class (N_Ci)	Landslide cell number in class (N_Li)	Frequency ratio, FR = [(N_Li/N_L)/(N_Ci/N_C)]	Class rates	Class weights (R)	General factor rates	General factor weights (W)	
Drainage density (m/km²)	0–100	1	30.6992	306992	11	0.1429	1	0.037	0.1343	9	0.0049691
ΣFr = 39.3	100–200	2	22.2849	222849	39	0.6979	5	0.1852			0.02487236
CI = 0	200–300	3	17.8869	178869	35	0.7803	5	0.1852			0.02487236
CR = 0	300–400	4	8.1161	81161	47	2.3092	7	0.2593			0.03482399
Table value = 1.49	400–536	5	0.7655	7655	68	35.4224	9	0.333			0.0447219
	No data		0.0487	487	0	0.0000					
Distance to drainage (m)	0–100	1	24.0518	240518	141	2.3368	9	0.333	0.02986	2	0.00994338
ΣFr = 3.66	100–200	2	20.1120	201120	28	0.5549	7	0.2593			0.0077427
CI = 0	200–300	3	15.9968	159968	25	0.6229	7	0.2593			0.0077427
CR = 0	300–500	4	16.0852	160852	6	0.1487	3	0.1111			0.00331745
Table value = 1.49	500–916	5	3.4752	34752	0	0.0000	1	0.037			0.00110482
	No Data		0.0803	803	0	0.0000					
Geological units	Al	1	0.3007	3007	1	1.3262	5	0.1641	0.08955	6	0.01469516
ΣFr = 13.74	Cy	4	2.1520	21520	0	0.0000	1	0.00074			6.6267E − 05
CI = 0.09177	Cyk	5	3.8384	38384	1	0.1039	2	0.14138			0.01266058
CR = 0.06159	Da	6	4.3703	43703	102	9.3072	9	0.24944			0.02233735
Table value = 1.49	Dag	7	1.6708	16708	1	0.2387	5	0.0966			0.00865053
	JKs	8	0.2667	2667	0	0.0000	1	0.0328			0.00293724
	KPt	9	13.9608	139608	94	2.6850	5	0.1379			0.01234895
	Ktüs	10	0.0263	263	0	0.0000	1	0.0378			0.00338499
	Ktüs	11	0.0598	598	0	0.0000	1				0
	Md	12	1.4808	14808	0	0.0000	1				0
	Mk	13	0.3962	3962	0	0.0000	1				0
	Pa	14	4.7285	47285	1	0.0843	2	0.0674			0.00603567
	Pk	15	0.9555	9555	0	0.0000	1				0
	Pka	16	1.4021	14021	0	0.0000	1	0.03978			0.0035623
	TRhk	17	25.0765	250765	0	0.0000	1				0
	TrrHz	18	3.9278	39278	0	0.0000	1				0
	Trhzb	19	6.6849	66849	0	0.0000	1				0

Table 3 continued

Factor	Range of class	Class no	Fr				AHP				Weights (R × W)
			Area of class (km²) (N_Li)	Cell number of class (N_Ci)	Landslide cell number in class (N_Li)	Frequency ratio, FR = [(N_Li/N_L)/(N_Ci/N_C)]	Class rates	Class weights (R)	General factor rates	General factor weights (W)	
Fault density (m/ km²)	Trg	20	3.4349	34349	0	0.0000	1				0
	Trgt	21	4.7841	47841	0	0.0000	1				0
	Trk	22	0.1381	1381	0	0.0000	1				0
	No Data		0.1461	1461	0	0.0000					
	0–100	1	54.8645	548645	113	0.8211	5	0.2381	0.044776	3	0.01066117
Σ Fr = 5.6	100–200	2	12.8609	128609	27	0.8369	5	0.2381			0.01066117
CI = 0	200–300	3	6.8437	68437	55	3.2038	9	0.4286			0.01919099
CR = 0	300–400	4	4.0385	40385	4	0.3948	1	0.04762			0.00213223
Table value = 1.49	400–571	5	1.1219	11219	1	0.3553	1	0.04762			0.00213223
	No Data		0.0718	718	0	0.0000					
Distance to fault (m)	0–250	1	27.6123	276123	96	1.3858	8	0.3279	0.02985	2	0.00978782
Σ Fr = 3.66	250–500	2	16.4587	164587	11	0.2664	2	0.081991			0.00244743
CI = 0.084	500–100	3	18.7426	187426	68	1.4462	9	0.3689			0.01101167
CR = 0.056	1000–1500	4	11.6816	116816	25	0.8531	5	0.1564			0.00466854
Table value = 1.49	1500–2233	5	5.2258	52258	0	0.0000	1	0.0647			0.0019313
	No Data		0.0803	803	0	0.0000					
Landuse Σ Fr = 20.96	Settlement	1	1.5315	15315	31	8.0714	7	0.2593	0.10448	7	0.02709166
	Dry agriculture	2	0.4369	4369	0	0.0000	1	0.037			0.00386576
CI = 0	Pasture	3	2.0397	20397	6	1.1730	5	0.1852			0.0193497
CR = 0	Forest	4	5.1580	51580	150	11.5962	9	0.3333			0.03482318
Tabe value = 1.24	İrrigation agriculture	5	9.4705	94705	1	0.0421	2	0.074			0.00773152
	Rocks	6	61.0141	610141	12	0.0784	3	0.1111			0.01160773
	No data		0.1506	1506	0	0.0000					

CI, CR and Table values are between 0–0.5, 0–0.86 and 0.58–1.49, respectively

Springer
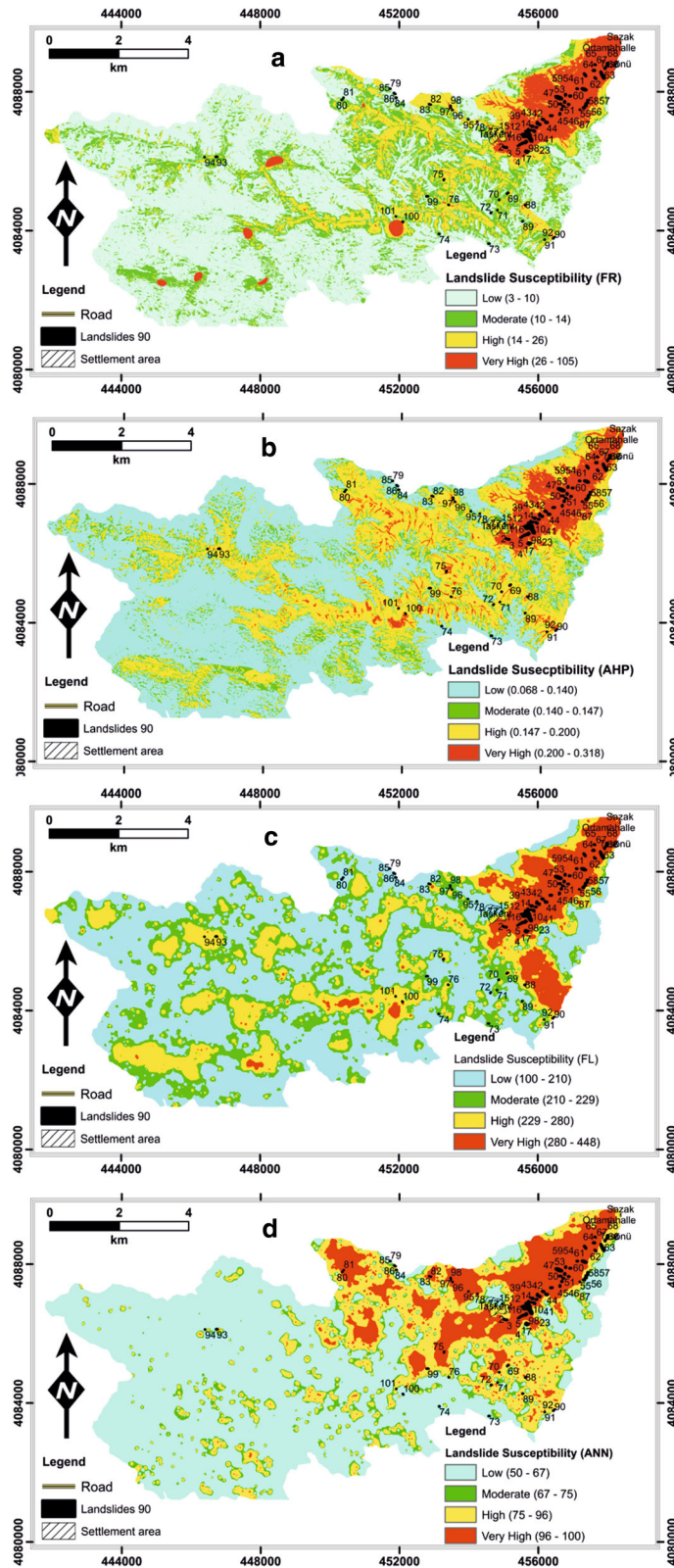
◀ **Fig. 5** Landslide susceptibility maps **a** FR model; **b** AHP model; **c** FL model; and **d** ANN model

sine, logistic (sigmoid), hyperbolic, and square root. The Multi-Layer Perceptron (MLP) with a feed-forward Back-error Propagation (BP) type of learning algorithm is a commonly used and are widely available neural network structure in the geospatial analysis (Pradhan et al. 2010a). Modelling of complex and nonlinear functions can be done through MLPs (Mousavi et al. 2016). The BP algorithm randomly selects the initial weights, and then compares the calculated output for a given observation with the expected output for that observation (Pajanowski et al. 2002). The differences between the expected and calculated output values across all observations are summed up using a loss function. After all observations are presented to the network, the weights are modified according to a generalized delta rule (Rumelhart et al. 1986), so that the total error is distributed among the various nodes in the network. These processes of feeding forward the features and back-propagating the errors are repeated iteratively (in some cases, many thousands of times) until the error stabilizes at a low level (Pajanowski et al. 2002).

According to the Chauhan et al. (2010) "there are three stages involved in ANN data processing for a classification problem: the training stage, the weight determination stage, and the classification stage. The training process is initiated by assigning arbitrary values to the connection weights which are constantly updated until an acceptable training accuracy is reached." The details of the method were given by Paola and Schowengerdt (1995), and Atkinson and Tatnall (1997).

The method was used to the determination prediction of LS in four phases: (1) designing of the network and preparing the inputs data; (2) training the network using the training set; (3) testing the network using the test data set; and (4) using the information from the neural network to forecast landsliding. For this study, the neural networks were constructed using the neural network toolbox of MATLAB (Pao 1999).

In this study, similar to the earlier studies (e.g., Nelson and Illingworth 1990; Haykin 1994; Masters 1994; Dowla and Rogers 1995; Looney 1996; Swingler 1996; Chauhan et al. 2010), we used 70% of the samples in the dataset as the training and 30% as

the test sets.. The dataset consisted of 377 points denoting the presence and the absence of landslides. 263 points (200 landslide and 63 non-landslide points), 70% of the dataset) were kept for training (Table 2). The MLP_BP learning algorithm is preferred for the analyses. Learning rate and momentum factor were selected as 0.01 and 0.9, respectively (Polykretis and Chalkias 2018).

Detailed information on the application of the method to LS studies can be obtained from Aleotti et al. (1996), Mayoraz et al. (1996), Lee et al. (2001), Fernandez-Steeger et al. (2002), Ermini et al. (2005) and Bartolomei et al. (2006).

In this study, 14 inputs, 28 hidden, and 1 output neuron structure has been used for the network (Fig. 6). The initial weights were randomly selected. The numbers of epochs in the software were set to 2000, and the root mean square error (RMSE) goal for the convergence criterion was set to 0.01. All of the iterations satisfied the 0.01 root mean square error condition with 2000 epochs. After the training, the model become ready to be used for the study area.

Finally, the LS map was prepared using the training set (Fig. 5d). The values were classified and grouped into four equal areas (first highest 10%, second highest 10%, third highest 20% and the remaining 60%) for visual interpretation. Some properties related to the application of artificial neural networks are also given in Table 4.

5000 points were randomly generated for the study area. The produced 5000 points were crossed with 14 factor maps and values of 5000 points on the factor maps have been determined. The newly determined (= 5000 × 14) 70000 data points were used in the simulations performed by the trained network. The sensitivities of the landslides corresponding to 5000 points were determined from the artificial neural network. The determined 5000 data points were interpolated to create a LS map (Fig. 5d). LS map was classified into 4 classes of LS regions: very low (no LS), low, medium and high.

3.3.4 Fuzzy Logic (FL) and Its Application to Landslide Susceptibility

In this paper, LS in the basin of Taşkent was also examined using fuzzy logics. For this purpose, reasoning engine named Mamdani has been utilized. Using the factors controlling the formation of
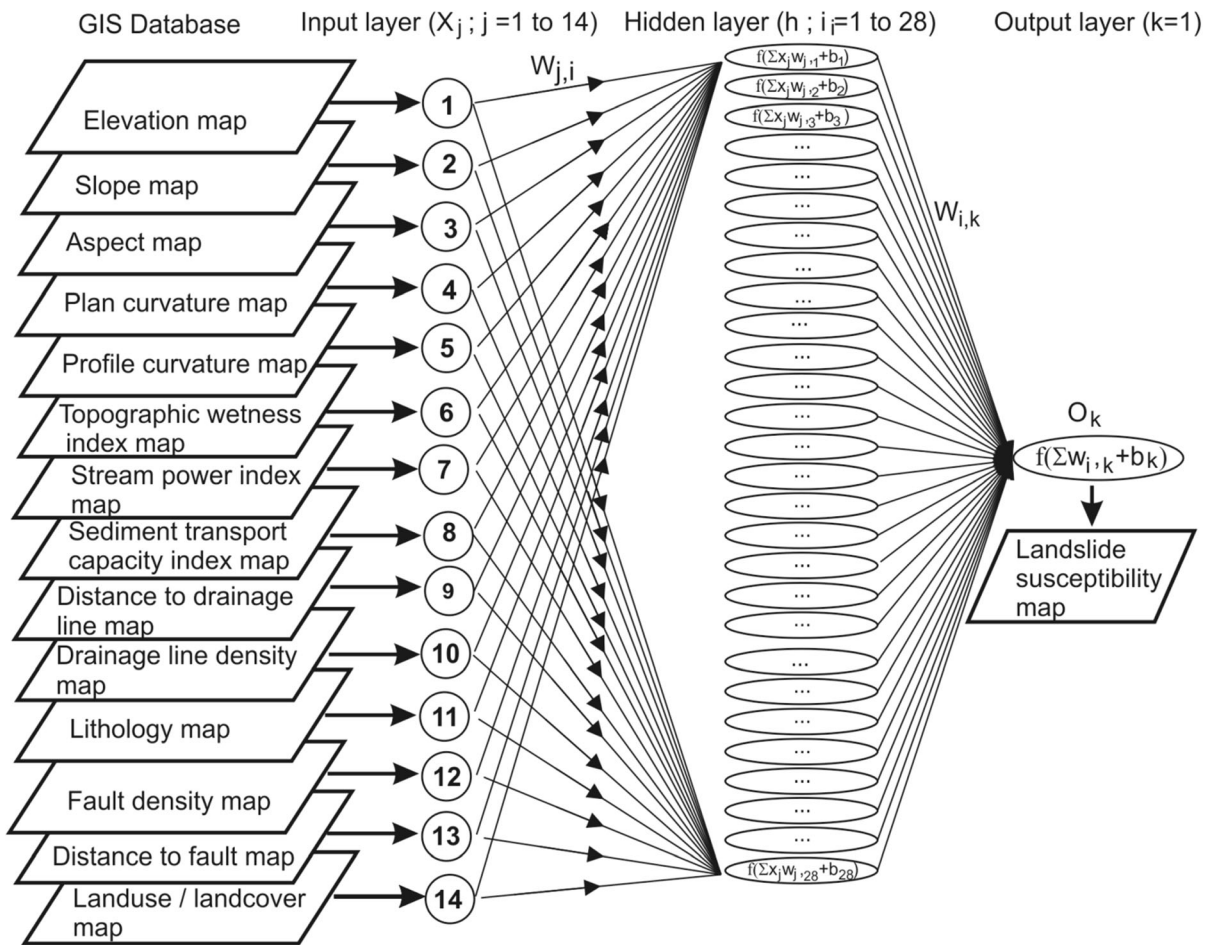
Fig. 6 Input and output layers of the ANN network

Table 4 ANN model characteristics used	Number of hidden layer nerons used	28
	Input layer data	EGS (263 × 14)
	Output layer data	ECS (263 × 1)
	Training function	TrainLM
	Adaptation learning	MSE
	Number of layers	3
	Transfer function	LOGSIG
	Used data	EGS: 263 and ECS: 263

landslides given above, LS map is also created by Fuzzy Logic (FL) model. The analyses were performed using MATLAB fuzzy toolbox and GIS software.

According to the Karkazi et al. (2001) "in order to solve a problem using a knowledge-based fuzzy system, it is necessary to describe and process the influencing factors in Fuzzy terms and provide the result of these processes in a usable form." The application steps of this method are given by Mendel (1995) as follows: "The basic elements of a knowledge-based FL consist of four major parts: (1) fuzzier,

(2) rules, (3) inference engine, and (4) defuzzifier. Firstly, a crisp set of input data are gathered and converted to a fuzzy set using fuzzy linguistic variables, fuzzy linguistic terms and membership functions. The assignment of a membership function to every variable of the problem is called fuzzification process." The concept of the linguistic variable illustrates particularly and clearly how fuzzy sets can form the bridge between linguistic expression and numerical information (Karkazi et al. 2001). This step is known as fuzzification. Membership functions are used in the fuzzification and defuzzification steps of a FLS, in order to map the non-fuzzy input values to fuzzy linguistic terms and vice versa. A membership function is used to quantify a linguistic term. There are different forms of membership functions such as triangular, trapezoidal, piecewise linear, Gaussian, or singleton (Saraswathi and Senthil 2017). However, the most common types of membership functions are triangular, trapezoidal, and Gaussian shapes. The type of membership function can be context dependent and is generally chosen arbitrarily according to the user experience (Mendel 1995). The functions used in the production of Fuzzy membership values are given in Eastman (2006).

In this study, the triangle shape was selected for all the membership functions after several trials and errors to find out the best function shape. Using the FR coefficients and the identified landslides, the fuzzy membership functions were constructed. The second step in this method is to determine how the inputs and outputs are connected to each other. A fuzzy rule is a simple IF–THEN rule with a condition and a conclusion. The evaluations of the fuzzy rules and the combination of the results of the individual rules are performed using fuzzy set operations." Zimmerman (1996) discussed a variety of combination rules, and Bonham-Carter (1994) discussed five operators, namely the fuzzy and, fuzzy or, fuzzy algebraic product, fuzzy algebraic sum and fuzzy gamma operator. The mostly- used operations for OR and AND operators are max and min, respectively (Mendel 1995). This study uses the fuzzy OR operator for combining the fuzzy membership functions. After the inputs were fuzzified, If–Then rules have been assigned (Riad et al. 2011). These if–then rule statements are used to formulate the conditional statements that comprise fuzzy logic (Pao 1999). 112 rules (if–then) were assigned in this study, Fuzzy OR operator was used in all the rules. After the inference step, the overall result should be defuzzified to obtain a final crisp output. Defuzzification is performed according to the membership function of the output variable (Alreshoodi et al. 2015). There are different algorithms for defuzzification. The frequently used algorithms are Center of Gravity, Center of Gravity for Singletons, Left Most Maximum, and Right Most Maximum (Mendel 1995). The most popular defuzzification method which was also applied in here is the centroid calculation which returns the center of the area under the curve. As a result of the analysis, a map showing the calculated fuzzy values was provided. These fuzzy values have been "defuzzyfied" into different LS levels. Defuzzyfication means to translate the calculated fuzzy values back to the "real world" (Schernthanner 2007). In LS mapping, fuzzy logic defines the instability factors as members of a set ranging from 1, expressing the highest susceptibility, to 0, expressing no susceptibility of landsliding, allowing different degrees of membership (Schernthanner 2007). Finally, the produced map (Fig. 5c) was compared with the existing landslide location map for verification of the prediction accuracy.

4 Validation of the Models

The validity of the produced LS maps was checked by test landslides which were not used in the production of LS maps. Again, the Receiver Operating Characteristics (ROC) curves method was used in the comparison process. As a result of this comparison, the performances of the LS maps produced by different methods were determined.

ROC values are obtained by plotting the cumulative True Positive Rates (TPR = sensitivity) versus False Positive Rate (FPR = 1–specificity) for each model (Marjanovic and Caha 2011). Figure 7 shows the ROC curve of the FR, FL, AHP and ANN model. The AUC values of the ROC curve obtained from FR, ANN, AHP, and FL models were found to be 0.926, 0.916, 0.899, and 0.842, respectively, with estimated standard errors between 0.023 and 0.039 (Fig. 7, Table 5). LS map produced with FR model has higher accuracy. The models evaluated in this study had a quite reasonable performance considering the results of the similar studies available in the literature (Kanungo et al. 2006; Oh and Lee 2010; Pradhan and Lee
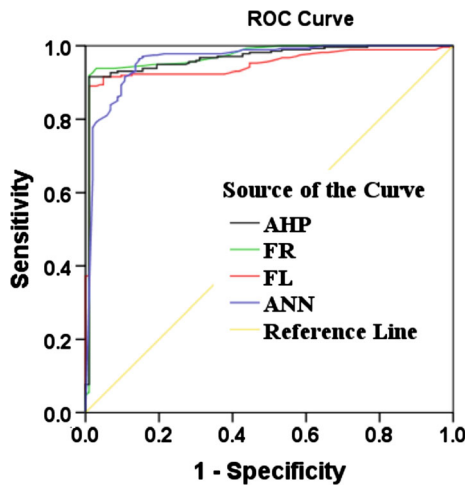
Fig. 7 ROC curves of the FR, FL, AHP and ANN model

Fig. 8 The distribution of the produced landslide susceptibility classes of test, analysis and all landslides

2010a, 2010b; Yilmaz 2010). Obtaining a relatively better results using the FR method (AUC of 92.6%) compared to the other methods is also in agreement with previous studies.

The accuracy of the LS maps has been also checked by overlaying them with the landslide inventory map. Locations of landsides have been intersected with the susceptibility maps and the number of coincident landslides was determined for each susceptibility class. A landslide was classified as the ''correct'' prediction when at least a part of it was located within a high or very high probability zone (Dai and Lee 2002). Otherwise, the prediction was considered as the ''wrong'' one. The 58 test landslides (76 pixels), 43 training landslides (200 pixels), and 101 total landslides (276 pixels), were overlaid onto the LS maps produced, and the existing landslide pixels within the different landslide occurrence potential classes were determined. The results of these inspections are given in Fig. 8. The results obtained by overlaying the predicted LS maps produced by AHP, FR, FL, and

ANN methods onto all existing landslides, indicated that 87%, 83%, 89%, and 76% of the observed landslides were concentrated in the high and very high LS classes, respectively (Fig. 8). For the test landslides, these percentages were 74%, 60%, 87%, and 33% for AHP, FR, FL, and ANN methods, respectively. During the validation process, it was shown that 93%, 91%, 89%, and 93% of the training or analysis landslides were predicted correctly, as shown in Fig. 8. Poudyal et al. (2010) found that the accuracies of the LS maps produced by the frequency ratio and neural networks methods had been 82.21 and 78.25%,

Table 5 Area under the curve	Test result variable(s)	Area	SE[a]	Asymptotic sig.[b]	Asymptotic 95% CI	
					Lower bound	Lower bound
	AHP	0.899	0.029	0.000	0.842	0.955
	FR	0.926	0.023	0.000	0.880	0.972
[a] Under the nonparametric assumption; [b] Null hypothesis; true area = 0.5	FL	0.842	0.039	0.000	0.766	0.918
	ANN	0.916	0.025	0.000	0.868	0.965

Table 6 Matrix of correlation coefficients obtained from the comparison of landslide susceptibility maps produced by different methods

Layer	AHP	FR	FL	ANN
AHP	1	0.82	0.63	0.54
FR	0.82	1	0.7	0.48
FL	0.63	0.7	1	0.45
ANN	0.54	0.48	0.45	1

respectively. In addition, the validation results of the study by Mohammady et al. (2012) showed that "the prediction accuracy of the Frequency Ratio, Dempster–Shafer, and Weights of Evidence models had been 80.13%, 78.32%, and 74.60% respectively." In the determination of landslide sensitivity, The FR method was found to be reliable.

The LS maps produced by different models have also been compared with each other (Table 6). Pearson's correlation coefficients for AHP versus FR, AHP versus FL, and AHP versus ANN were found to be 0.82, 0.63, and 0.54, respectively. The correlation coefficients were found to be 0.70 and 0.48 for FR versus FL and FR versus ANN maps, respectively. The correlation coefficient was found to be 0.45 for FL versus ANN map. Interpretations of correlation coefficients are given by ILWIS, (2001). According to this definition, if the correlation coefficient is between 0–0.2, 0.2–0.4, 0.4–0.7, 0.7–0.9, and 0.9–1, the correlation is evaluated as very weak, weak, medium, high and very high, respectively. As can be seen from the results, there are high correlations between the maps produced by FR-AHP, and FR-FL methods. The susceptibility map produced by the ANN model was compared with the susceptibility maps produced by other models. As a result of this comparison, the relationship was found to be weak. It is evaluated that the low number of landslides (the small of the training set) can be effective in the poor performance of the ANN method. Detailed information on increasing the performance of the ANN method can be obtained from Mousavi et al. (2016) and Pradhan and Lee (2010a). However, when the LS map produced by the FR model was compared with the sensitivity maps produced with other models, it was found that the correlation coefficient was high.

5 Results and Discussions

In this study, four models: (1) the FR, (2) the AHP, (3) the ANN, and (4) the FL have been used to derive the relationships between the landslide distribution and the landslide conditioning factors. The existing and produced landslide inventory maps were compared to each other for the verification of the results. Details of this LS map comparison have been described and given below (Fig. 9a–n).

Many landslides occurred at the elevations between 1063 and 1508 m, concentrated at elevations between 1063 and 1317 m (Fig. 9a). There are no or few landslides at elevations between 1508 and 1961 m. The results were dependent on the geology of the investigated area. In this area, the elevation is in a range of 1063–1508 m. The rocks in this area are generally volcanic rocks with high strength.

Many landslides occurred in the study area at slopes between 14° and 33° (Fig. 9b). There are no or few landslides at gentle (slope angle < 6°) and steep slopes (slope angle > 43°). Due to the small shear stresses, landslides are less common on the gentle slopes (Lee and Talib 2005). The shear stresses increase with increasing slope angle. On very steep slopes, there is generally no soil; there is a high-strength rock.

Therefore the landslide susceptibility of these slopes are low (Jones et al. 1961; Pradhan 2010a, b). The 14°–33° slope categories were the most unstable areas in the study area. It can be explained by the fact that most of the geological units with low strength were outcropped at slope angles between 14° and 33°.

Based upon the landslide distribution, the slopes facing South (113–203) and North (293–338) were considered being prone to landslides more than the others. This condition may be caused by the humidity (Fig. 9c).

Profile curvature affects the acceleration and deceleration of flow across the surface (Fig. 9e). Plan curvature affects the convergence and divergence of flow across the surface (Fig. 9d). The landslides in the study area typically had more tendencies to occur in curvature areas with a negative plan (convergence) and with negative profile (convex). The convex areas in the study possess higher LS values than the other areas possess due to curvature. Convex slopes can be exposed to repeated dilation and contraction of loose debris on an inclined surface that can induce creeping
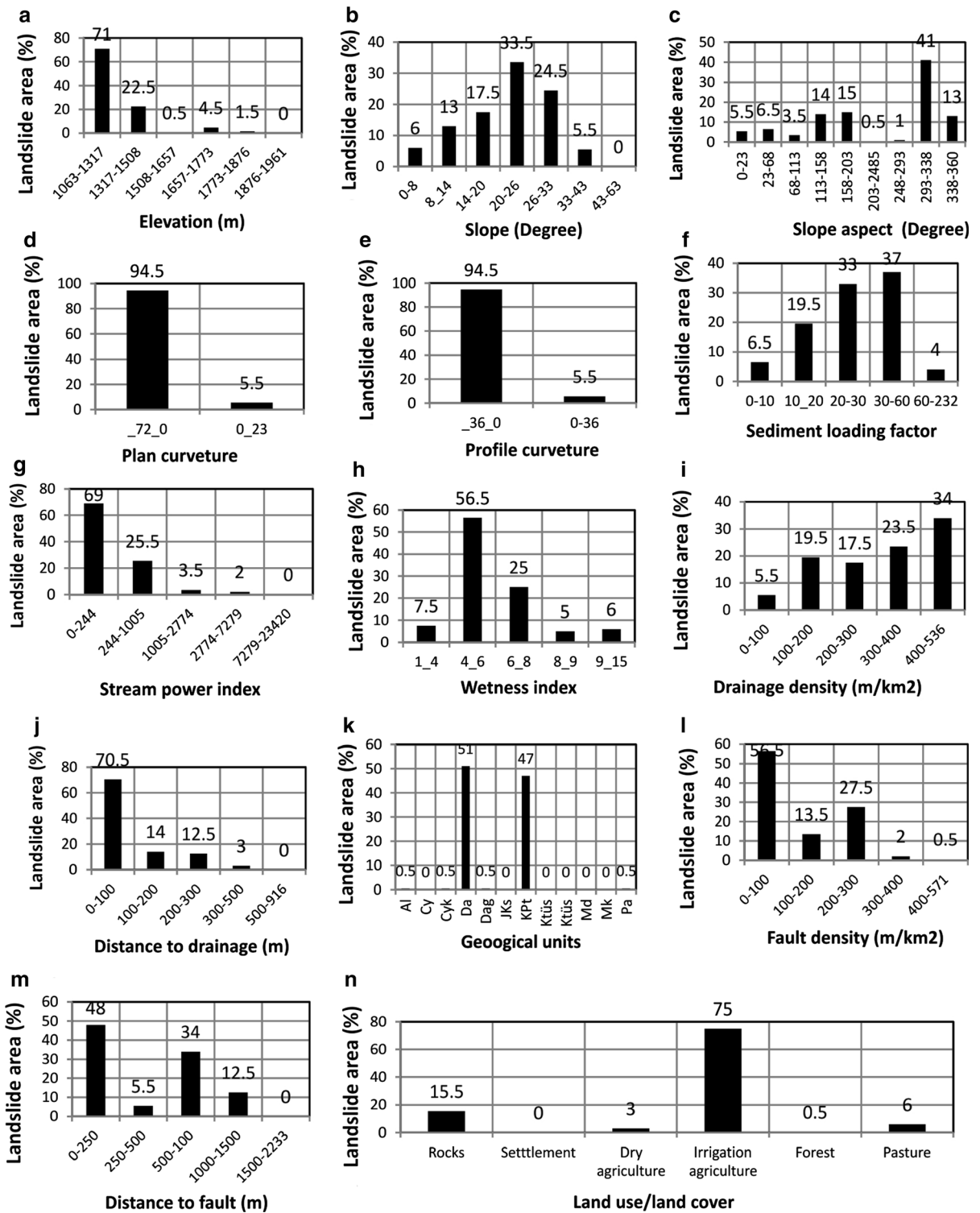
Fig. 9 Distribution of landslides into the classes of conditional factors

or a mudslide due to heavy rainfall (Pradhan 2011). On the other hand, the results of this study are in agreement with those of Havenith et al. (2006), where the following conclusions were made:" (1) landslide scars match convex areas well (Conforti et al. 2012). (2) Convex slopes are less stable under similar hydrogeological conditions (lower factor of safety) because a larger body (larger driving force) is acting on the same sliding surface (equal resistant forces). (3) Convex morphologies might indicate the presence of accumulation material (colluvium) that is characterized by lower shear resistance (Havenith et al. 2006).

LS is higher in areas where the STI ranges from 10 to 60 and lower in areas where the index values are between 0–10 and 60–232 (Fig. 9f). On the other hand, it is determined that landslides are abundant more at the classes of low STI index values than in other classes. In the case of using a stream power index (Fig. 9g), the landslide occurrence was higher for lower stream power index values. High TWI values indicate areas that are more likely (higher probability) to drain by the saturated excess flow. Threshold values for classifying areas where saturation excess overland flow will occur, though based on empirical soil properties, are 0.6 (normalized value) and above (Leh et al. 2008). The landslides had more tendency to occur TWI values between 4 and 8 (0.26–0.53 normalized). For lower or higher values of wetness index, the LS areas are small, whereas for middle values, the areas are large (Fig. 9h). As for the relationship between landslide occurrence and distance from the faults, the landslide frequency generally decreases with increasing distance from fault (Fig. 9m). This study indicates that most landslides occur within a fault distance of 0–250 m, whereas previous studies suggested that most landslides occur within a fault distance of 250–1000 m (Gupta and Joshi 1990; Gokceoglu and Gokceoglu 1996; Pachauri et al. 1998). Khanh (2009) concluded that landslides are more in the zone where the distance to faults is between 250 and 1000 m. However, there are many researchers who state that this determination may not be accurate for every place and every terrain (Gemitzi et al. 2010; Uromeihy and Mahdavifar 2000). The distance to the drainage map shows that landslides are closely located within the 100 m buffer zone (Fig. 9j). As for the relationship between landslide occurrence and the distance from drainage, the landslide frequency generally decreases with the increasing

distance from a drainage line. A distance of less than 100 m indicates a high probability of landslide occurrence, whereas distances more than 300 m indicates a low probability. Dai et al. (2001a) has also indicated that "streams can adversely affect the stability by eroding slopes or saturating the lower part of the material until the water level increases. Intarawichian and Dasananda (2011) have concluded that "landslide occurrence probability is high in areas where the distance to drainage is between 1500 and 2000 m and the landslides are likely to occur most often at specific distances from the drainage." Fourniadis et al. (2007) most likely drew the same conclusion after observing the terrain modification caused by gully erosion and the undercutting of slopes in the study area that might have influenced the initiation of landslides. The fault density values are found to vary between zero and 400.5 m/km^2. It is determined that many of the landslides are located in the 0–300 m/km^2 fault density zone (Fig. 9l). In the study area, it was determined that there is a linear relationship between drainage density and landslide formation (Fig. 9i). This result is suitable with the findings of Sarkar and Kanungo's (2004). In mountainous regions, drainage density provides an indirect measure of groundwater conditions which have an important role to play in landslide activity (Sarkar and Kanungo 2004). Landslides are mostly formed in agriculture areas (Fig. 9n). It was determined that the formation of the landslides decreased with the increase in altitude, sediment loading factor, plan curvature, profile curvature, stream power index, distance to drainage, distance to fault, and fault density values. The formation of the landslides is found to increase up to a certain slope, sediment loading factor, and wetness index value, but then decline. Many landslides were formed in Aslakyayla (Da) and Taşkent (KPt) formations (Fig. 9k).

The generated LS maps are divided into 4 subclasses, low, medium, high and very high susceptibility classes. Landslides were also divided into two subclasses as test and analysis landslides. The distribution of the landslides, all the landslides, the test landslides that are not used in the analysis, and the analysis landslides that are used for the analysis are given in Fig. 8 according to the landslide subclasses. It has been determined that 87%, 83%, 89% and 76% of the analysis landslides are located in the high-to-high LS subclasses indicated in the LS maps produced by

the AHP, FR, FL and ANN methods, respectively. It was also determined that 74%, 60%, 88% and 33% of the test landslides are located in the high-to-high LS subclasses indicated in the LS maps produced by the AHP, FR, FL and ANN methods, respectively. Similarly, It was also determined that 93%, 91%, 89% and 93% of the analysis landslides are located in the high-to-high LS subclasses indicated in the LS maps produced by the AHP, FR, FL and ANN methods, respectively (Fig. 8).

6 Conclusions

In this study, LS maps were created with four different methods, FR, FL, AHP and ANN, using the data obtained from the same field. The accuracy of the produced susceptibility maps was tested. The highest ROC value was obtained from the sensitivity map produced by the FR method, whereas the lowest ROC value was obtained from the map generated by the FL method. Later on, LS maps produced by different methods were compared with each other. It has been determined that the highest and lowest correlation values were obtained for FR and AHP correlation as 0.82, and ANN and FL correlation as 0.45, respectively. Following these evaluations, it was found out that it was more appropriate to apply the FR as the primary and the AHP as the secondary method in the production of the LS maps. Meanwhile, the FR method is simple, can be easily implemented, and provides very high accuracy. The accuracy comparison of the FR method with LR and WOE methods in the production of the LS maps was performed by Ozdemir and Altural (2013). They found out that the FR method produces more consistent results than the others. As a result, it is recommended to use the FR method in LS studies.

References

Akgun A (2012) A comparison of landslide susceptibility maps produced by logistic regression, multi-criteria decision, and likelihood ratio methods: a case study at İzmir, Turkey. Landslides 9:93–106. https://doi.org/10.1007/s10346-011-0283-7

Akgun A, Dag S, Bulut F (2008) Landslide susceptibility mapping for a landslide-prone area (Findikli, NE of Turkey) by likelihood-frequency ratio and weighted linear combination models. Environ Geol 54:1127–1143

Aleotti P, Balzelli P, De Marchi D (1996) Le reti neurali nella valutazione della suscettibilita' da frana. Geol Tecnica Ambient 5(4):37–47

Alreshoodi M, Danish E, Woods J, Fernando A, Alwis CD (2015) Prediction of perceptual quality for mobile video using fuzzy inference systems. IEEE Trans Consum Electron 61(4):546–554

Anbalgan R (1992) Landslide hazard evaluation and zonation mapping in mountainous terrain. Eng Geol 32:269–277

Atkinson PM, Tatnall ARL (1997) Neural networks in remote sensing. Int J Remote Sens 18:699–709

Ayalew L, Yamagishi H (2005) The application of GIS-based logistic regression for landslide susceptibility mapping in the Kakuda-Yahiko Mountains, Central Japan. Geomorphology 65:15–31

Ayalew L, Yamagishi H, Ugawa N (2004) Landslide susceptibility mapping using GIS-based weighted linear combination, the case in Tsugawa area of Agano River, Niigata prefecture, Japan. Landslides 1:73–81

Ayalew L, Yamagishi H, Marui H, Kanno T (2005) Landslides in Sado Island of Japan: part II. GIS-based susceptibility mapping with comparisons of results from two methods and verifications. Eng Geol 81:432–445

Ayenew T, Barbieri G (2005) Inventory of landslides and susceptibility mapping in the Dessie area, northern Ethiopia. Eng Geol 77(1–2):1–15

Barredo JI, Benavidesz A, Herhl J, Van Westen CJ (2000) Comparing heuristic landslide hazard assessment techniques using GIS in the Tirajana basin, Gran Canaria Island, Spain. Int J Appl Earth Obs Geoinf 2:9–23

Bartolomei A, Brugioni M, Canuti P, Casagli N, Catani F, Ermini L, Kukavicic M, Menduni G, Tofani V (2006) Analisi della suscettibilità da frana a scala di bacino (Bacino del Fiume Arno, Toscana-Umbria, Italia). Giornale Geol Appl 3(2006):189–195. https://doi.org/10.1474/GGA.2006-03.0-25.0118

Bathurst JC, Bovolo CI, Cisneros F (2010) Modelling the effect of forest cover on shallow landslides at the river basin scale. Ecol Eng 36(3):317–327

Begueria S (2006) Validation and evaluation of predictive models in hazard assessment and risk management. Nat Hazards 37:315–329

Bonham-Carter GF (1994) Geographic information systems for geoscientists: modeling with GIS. Pergamon Press, Ottawa, p 398

Brenning B (2005) Spatial prediction models for landslide hazards: review, comparison and evaluation. Nat Hazards Earth Syst Sci 5:853–862

Cannon SH (2000) Debris-flow response of southern California watersheds burned by wildfire. In: Wieczorek GF, Naeser ND (eds) Debris-flow hazards mitigation, mechanics, prediction and assessment. Balkema, Rotterdam, pp 45–52

Cevik E, Topal T (2003) GIS-based landslide susceptibility mapping for a problematic segment of the natural gas pipeline, Hendek (Turkey). Environ Geol 44(8):949–962

Chauhan S, Sharma M, Arora MK, Gupta NK (2010) Landslide susceptibility zonation through ratings derived from artificial neural network. Int J Appl Earth Observ Geoinf 12:340–350

Chen CH, Ke CC, Wang CL (2009) A back-propagation network for the assessment of susceptibility to rock slope failure in the eastern portion of the Southern Cross-Island Highway in Taiwan. Environ Geol 57:723–733

Clerici A, Perego S, Tellini C, Vescovi P (2006) A GIS-based automated procedure for landslide susceptibility mapping by the Conditional Analysis method: the Baganza valley case study (Italian Northern Apennines). Environ Geol 50:941–961

Conforti M, Robustelli G, Muto F, Critelli S (2012) Application and validation of bivariate GIS-based landslide susceptibility assessment for the Vitravo river catchment (Calabria, south Italy). Nat Hazards 61(1):127–141

Dahal RK, Hasegawa S, Nonomura S, Yamanaka M, Masuda T, Nishino K (2008) GIS-based weights-ofevidence modelling of rainfall-induced landslides in small catchments for landslide susceptibility mapping". Environ Geol 54(2):314–324

Dai FC, Lee CF (2002) Landslide on natural terrain-physical characteristics and susceptibility mapping in Hong Kong. Mt Res Dev 22(1):40–47

Dai F, Lee C, Li J, Xu ZW (2001a) Assessment of landslide susceptibility on the natural terrain of Lantau Island, Hong Kong. Environ Geol 40:339–381. https://doi.org/10.1007/s002540000163

Dai FC, Lee CF, Xu ZW (2001b) Assessment of landslide susceptibility on the naturalte rrain of Lantau Island, Hong Kong. Environ Geol 40(3):381–391

Daneshvar MRM, Bagherzadeh A (2010) The feasibility of landslide susceptibility map with using GIS at Golmakan Watershed. The 1st International Applied Geological Congress, Department of Geology, Islamic Azad University-Mashad Branch, Iran, 26–28 April 2010

Dowla FU, Rogers LL (1995) Solving problems in environmental engineering and geosciences with artificial neural Networks. The MIT Press, London

Eastman JR (2006) IDRISI Andes guide to GIS and image processing. Clark University, USA, Clark Labs

Ercanoglu M, Gokceoglu C (2002) Assessment of Landslide Susceptibility for a Landslide-Prone Area (north of Yenice, NW Turkey) by Fuzzy Approach. Environ Geol 41:720–730

Ermini L, Catani F, Casagli N (2005) Artificial neural network applied to landslide susceptibility assessment. Geomorphology 66:327–343. https://doi.org/10.1016/j.geomorph.2004.09.025

Fernandez T, Irigaray C, El Hamdouni R, Chacon J (2008) Correlation between natural slope angle and rock mass strength rating in the Betic Cordillera, Granada, Spain. Bull Eng Geol Environ 67:153–164. https://doi.org/10.1007/s10064-007-0118-x

Fernandez-Steeger TM, Rohn J, Czurda K (2002) Identification of landslide areas with neural nets for hazard analysis. In: Stemberk J,Wagner P, Rybar J [eds] Landslides: proceedings of the first European conference on landslides, Prague, Czech Republic, June 24–26 2002, pp 163–168

Fourniadis IG, Liu JG, Mason PJ (2007) Landslide hazard assessment in the three Gorges area, China, using ASTER imagery: Wushan-Badong. Geomorphology 84:126–144

García-Rodríguez MJ, Malpica JA, Benito B, Díaz M (2008) Susceptibility assessment of earthquake-triggered landslides in El Salvador using logistic regression. Geomorphology 95:172–191

Gemitzi A, Falalakis G, Eskioglou P, Petalas C (2010) Evaluating landslide susceptibility using environmental factors, fuzzy membership functions and gis. Global Nest J 13(1):28–40

Glade T (2003) Vulnerability assessment in landslide risk analysis. Erde 134(2):123–146

Gokceoglu C, Gokceoglu H (1996) Landslide susceptibility mapping of the slopes in the residual soils of the Mengen region (Turkey) by deterministic stability analyses and image processing techniques. Eng. Geol 44:147–161

Gorsevski PV, Jankowski P, Gessler PE (2006) An heuristic approach for mapping landslide hazard by integrating fuzzy logic with analytic hierarchy process. Control Cybern 35:1

Gritzner ML, Marcus WA, Aspinall R, Custer SG (2001) Assessing landslide potential using GIS, soil wetness modeling and topographic attributes, Payette River, Idaho. Geomorphology 37(1–2):149–165

Gupta RP, Joshi BC (1990) Landslide Hazard Zonation using the GIS approach: A case study from the Ramganga Catchment, Himalayas. Eng Geol 28:119–131

Guzzetti F, Carrarra A, Cardinali M, Reichenbach P (1999) Landslide hazard evaluation: a review of current techniques and their application in a multi-scale study. Central Italy. Geomorphology 31:181–216

Havenith HB, Strom A, Caceres F, Pirard E (2006) Analysis of landslide susceptibility in the Suusamyr region, Tien Shan: statistical and geotechnical approach. Landslides 3:39–50

Haykin S (1994) Neural networks: a comprehensive foundation. Macmillan, New York

ILWIS (2001) ILWIS 3.0 academic user's guide. Aerospace Survey and Earth Sciences (ITC) Enschede, The Netherlands, 530 p

Intarawichian N, Dasananda S (2010) Analytical hierarchy process for landslide susceptibility mapping in Lower Mae Chaem Watershed, northern Thailand, Suranaree. J Sci Technol 17(3):1–16

Intarawichian N, Dasananda S (2011) Frequency ratio model based landslide susceptibility mapping in lower Mae Chaem watershed, Northern Thailand. Environ Earth Sci. https://doi.org/10.1007/s12665-011-1055-3

Jakob M (2000) The impacts of logging on landslide activity at Clayoquot Sound British Columbia. CATENA 38:279–300

Jones FO, Embody DR, Peterson WC (1961) Landslides along the Columbia river valley, Northeastern Washington, U.S. Geol Surv Prof Pap 367:1–98

Kanungo DP, Arora MK, Sarkar S, Gupta RP (2006) A comparative study of conventional, ANN black box, fuzzy and combined neural and fuzzy weighting procedures for landslide susceptibility zonation in Darjeeling Himalayas. Eng Geol 85:347–366

Kanungo DP, Arora MK, Gupta RP, Sarkar S (2008) Landslide risk assessment using concepts of danger pixels and fuzzy set theory in Darjeeling Himalayas. Landslides 5:407–416

Karkazi A, Hatzichristos T, Mavropoulos A, Emmanouilidou B, Elseoud A (2001) Landfill siting using GIS and fuzzy logic. EPEM S.A. Department of Solid and Hazardous Wastes, Greece; Egyptian Environmental Affairs Agency; and Dept. of Geography, National Technical University of

Athens, Greece. http://www.epem.gr/pdfs/2001_2.pdf. Accessed 22 Aug 2019

Khanh NQ (2009) Landslide hazard assessment in muonglay, Vietnam applying GIS and remote sensing. Dr.rer. nat. at the Faculty of Mathematics and Natural Sciences Ernst-Moritz-Arndt-University Greifswald. https://epub.ub.uni-greifswald.de/frontdoor/deliver/index/docId/661/file/khanh_thesis_final. Accessed 22 Aug 2019

Lan HX, Zhou CH, Wang LJ, Zhang HJ, Li RH (2004) Landslide hazard spatial analysis and prediction using GIS in the Xiaojiang watershed, Yunnan. China. Eng Geol 76(1–2):109–128

Lee S (2005a) Application of logistic regression model and its validation for landslide susceptibility mapping using GIS and remote sensing data. Int J Remote Sens 26:1477–1491

Lee S (2005b) Application and cross-validation of spatial logistic multiple regression for landslide susceptibility analysis. Geosciences 9(1):63–71

Lee S (2007) Comparison of landslide susceptibility maps generated through multiple logistic regression for three test areas in Korea. Earth Surf Proc Land 32:2133–2148

Lee S, Min K (2001) Statistical analysis of landslide susceptibility at Youngin, Korea. Environ Geol 40:1095–1113

Lee S, Pradhan B (2007) Landslide hazard mapping at Selangor, Malaysia using frequency ratio and logistic regression models. Landslides 4(1):33–41

Lee S, Sambath T (2006) Landslide susceptibility mapping in the Damrei Romel area, Cambodia using frequency ratio and logistic regression models. Environ Geol 50:847–855

Lee S, Talib JA (2005) Probabilistic landslide susceptibility and factor effect analysis. Environ Geol 47:982–990

Lee S, Ryu J, Min K, Won J (2001) Proceedings of the geoscience and remote sensing symposium IGARSS '01. In: IEEE 2001 international, vol 5, pp 2364–2366

Lee S, Ryu JH, Won JS, Park HJ (2004) Determination and application of the weights for landslide susceptibility mapping using an artificial neural network. Eng Geol 71:289–302

Leh MD, Chaubey I, Murdoch J, Brahana JV, Haggard BE (2008) Delineating runoff processes and critical runoff source areas in a Pasture Hillslope of the Ozark highlands. Hydrol Process 22:4190–4204

Lin ML, Tung CC (2003) A GIS-based potential analysis of the landslides induced by the Chi-Chi earthquake. Eng Geol 71:63–77

Lineback Gritzner M, Marcus WA, Aspinall R, Custer SG (2001) Assessing landslide potential using GIS, soil wetness modeling and topographic attributes, Payette River, Idaho. Geomorphology 37:149–165

Looney CG (1996) Advances in feedforward neural networks: demystifying knowledge acquiring black boxes. IEEE Trans Knowl Data Eng 8(2):211–226

Luzi L, Pergalani F (1999) Slope instability in static and dynamic conditions for urban planning: the ''Oltre Po Pavese'' case history (Region Lombardia-Italy). Nat Hazards 20:57–82

Magliuloü P, Lisio A, Russo F (2009) Comparison of GIS-based methodologies for the landslide susceptibility assessment. Geoinformatica 13(3):253–265. https://doi.org/10.1007/s10707-008-0063-2

Mahdavifar M (1997) Landslide susceptibility mapping in Khoresh Rostam area, Khalkhal, In: Proceedings of 2nd conference on landslide and damage mitigation, Tehran, May 5–6 1997

Marjanovic M, Caha J (2011) Fuzzy approach to landslide susceptibility zonation. In: V. Snasel, J. Pokorny, K. Richta (eds) Dateso 2011, pp. 181–195. ISBN:978-80-248-2391-1

Masters T (1994) Practical neural network recipes in C++. Academic Press, Boston

Mayoraz F, Cornu T, Vuillet L (1996) Using neural networks to predict slope movements. In: Proceedings of VII international symposium on landslides, Trondheim, June 1966, Balkema, pp 295–300

Meisina C, Scarabelli S (2007) A comparative analysis of terrain stability models for predicting shallow landslides in colluvial soils. Geomorphology 87:207–223

Melchiorre C, Matteucci M, Remondo J (2006) Artificial neural networks and robustness analysis in landslide susceptibility zonation. In: IEEE. 2006 international joint conference on neural networks Sheraton Vancouver Wall Centre Hotel, Vancouver, 16–21 July, pp 4375–4381

Melchiorre C, Matteucci M, Azzoni A, Zanchi A (2008) Artificial neural net- works and cluster analysis in landslide susceptibility zonation. Geomorphology 94:379–400

Melchiorre C, CastellanosAbella EA, vanWesten CJ (2010) Matteucci M (2010) Evaluation of prediction capability, robustness, and sensitivity in non-linear landslide susceptibility models, Guanta´namo, Cuba. Comput Geosci. https://doi.org/10.1016/j.cageo.2010.10.004

Mendel JM (1995) Fuzzy logic systems for engineering: a tutorial. IEEE Proc 83(3):345–377

Menendez Duarte R, Marqınez J (2002) The influence of environmental and lithologic factors on rockfall at a regional scale: evaluation using GIS. Geomorphology 43:117–136

Miner AS, Vamplew P, Windle DJ, Flentje P, Warner P (2010) A comparative study of various data mining techniques as applied to the modeling of Landslide susceptibility on the Bellarine Peninsula, Victoria, Australia. In: Geologically Active, Proceedings of the 11th IAEG congress of the international association of engineering geology and the environment, Auckland, New Zealand

Mohammady M, Moradi HR, Feiznia S, Pourghasemi HR (2010) Comparison of the efficiency of certainty factor, information value and AHP models in landslide hazard zonation (case study: part of Haraz Watershed). J Range Watershed Manag Iran J Nat Resour 62(4):539–551 (in Persian)

Mohammady M, Pourghasemi HR, Pradhan B (2012) Landslide susceptibility mapping at Golestan Province, Iran: a comparisonbetween frequency ratio, Dempster-Shafer, and weights-of-evidence models. J Asian Earth Sci 61(2012):221–236

Moore I, Gessler PE, Nielsen GA, Peterson GA (1993) Soil attribute prediction using terrain analyses. Soil Sci Soc Am J 57:443–452

Moradi M, Bazyar MH, Mohammadi Z (2012) GIS-based landslide susceptibility mapping by AHP method, a case study, Dena City, Iran. J Basic Appl Sci Res 2(7):6715–6723

Mousavi SM, Omidvar B, Ghazban F, Feyzi R (2011) Quantitative risk analysis for earthquake-induced landslides-Emamzadeh Ali. Iran. Eng Geol 122:191–203

Mousavi SM (2017) Landslide susceptibility in cemented volcanic soils, ask region. Indian Geotech J 47(1):115–130. https://doi.org/10.1007/s40098-016-0189-3

Mousavi SM, Horton SP, Langston CA, Samei B (2016) Seismic features and automatic discrimination of deep and shallow induced-microearthquakes using neural Network and logistic regression. Geophys J Int 207(1):29–46. https://doi.org/10.1093/gji/ggw258

Mousavi SM, Beroza GC, Hoover SM (2018) Variabilities in probabilistic seismic hazard maps for natural and induced seismicity in the Central and Eastern United States. Lead Edge 37(2):141a1–141a9. https://doi.org/10.1190/tle37020810.1

Muthu K, Petrou M, Tarantino C, Blonda P (2008) Landslide possibility mapping using fuzzy approaches. IEEE Trans Geosci Remote Sens 46:1253–1265

Mwasi B (2001) Land use conflicts resolution in a fragile ecosystem using Multi-Criteria Evaluation (MCE) and a GIS-based decision support system (DSS). In: International conference on spatial information for sustainable development, Nairobi, Kenya, October 2–5, 2001. http://www.iapad.org/wp-content/uploads/2015/07/mwasi-TS14-2.pdf

Nagarajan R, Roy A, Vinod Kumar R, Mukherjee A, Khire MV (2000) Landslide hazard susceptibility mapping based on terrain and climatic factors for tropical monsoon regions. Bull Eng Geol Environ 58:275–287

Nefeslioglu HA, Duman TY, Durmaz S (2008) Landslide susceptibility mapping for a part of tectonic Kelkit Valley (Eastern Black Sea region of Turkey). Geomorphology 94:401–418

Nelson M, Illingworth WT (1990) A practical guide to neural nets. Addison-Wesley, Reading

Nie H F, Diao S J, Liu J X, Huang H (2001) The application of remote sensing technique and AHP-fuzzy method in comprehensive analysis and assessment for regional stability of Chongqing City, China. In: Proceedings of the 22nd international asian conference on remote sensing, November 5–9, 2001. University of Singapore, Singapore, vol 1, pp 660–665

Oh H-J, Lee S (2010) Assessment of ground subsidence using GIS and the weightsof-evidence model. Eng Geol 115:36–48

Oh H, Lee S, Chotikasathien W, Kim CH, Kwon JH (2009) Predictive landslide susceptibility mapping using spatial information in the Pechabun area of Thailand. Environ Geol 57:641. https://doi.org/10.1007/s00254-008-1342-9

Ozdemir A (2009) Landslide susceptibility mapping of vicinity of Yakalandslide (Gelendost, Turkey)using conditional probability approach in GIS. Environ Geol 57:1675–1686

Ozdemir A, Altural T (2013) A comparative study of frequency ratio, weights of evidence and logistic regression methods for landslide susceptibility mapping: Sultan Mountains, SW Turkey. J Asian Earth Sci 64(2013):180–197

Pachauri AK, Pant M (1992) Landslide hazard mapping based on geological attributes. EngGeol 32:81–100

Pachauri AK, Gupta PV, Chander R (1998) Landslide zoning in a part of the Garhwal Himalayas. Environ Geol 36:325–334

Pajanowski BC, Brown DG, Shellito BA, Manik GA (2002) Using neural networks and gis to forecast land use changes: a land transformation model. Comput Environ Urban Syst 26(2002):553–575

Pao YC (1999) Engineering analysis, interactive methods and programs with FORTRAN, QuickBASIC, MATLAB, and mathematica. CRC Press, Boca Raton

Paola JD, Schowengerdt RA (1995) A review and analysis of backpropagation neural networks for classification of remotely sensed multi-spectral imagery. Int J Remote Sens 16:3033–3058

Paulin GL, Bursik M (2009) Logisnet: a tool for multimethod, multiple soil layers slope stability analysis. Comput Geosci 35:1007–1016

Pirasteh S, Pradhan B, Mahmoodzadeh A (2009) Stability mapping and landslide recognition in Zagros Mountain South West Iran: a case study. Disaster Adv 2(1):47–53

Polykretis C, Chalkias C (2018) Comparison and evaluation of landslide susceptibility maps obtained from weight of evidence, logistic regression, and artificial neural network models. Nat Hazards 93:249–274

Poudyal CP, Chang C, Oh HJ, Lee S (2010) Landslide susceptibility maps comparing frequency ratio and artificial neural networks: a case study from the Nepal Himalaya. Environ Earth Sci 61:1049–1064

Pourghasemi HR, Pradhan B, Gokceoglu C (2012) Application of fuzzy logic and analytical hierarchy process (AHP) to landslide susceptibility mapping at Haraz watershed, Iran. Nat Hazards 63:965–996

Pradhan B (2010a) Remote sensing and GIS-based landslide hazard analysis and cross-validation using multivariate logistic regression model on three test areas in Malaysia. Adv Space Res 45:1244–1256. https://doi.org/10.1016/j.asr.2010.01.006

Pradhan B (2010b) Application of an advanced fuzzy logic model for landslide susceptibility analysis. Int J Comput Intell Syst 3(3):370–381

Pradhan B, Lee S (2010c) Delineation of landslide hazard areas on Penang Island, Malaysia, by using frequency ratio, logistic regression, and artificial neural network models. Environ Earth Sci 60:1037–1054. https://doi.org/10.1007/s12665-009-0245-8

Pradhan B (2011) Manifestation of an advanced fuzzy logic model coupled with Geo-information techniques to landslide susceptibility mapping and their comparison with logistic regression modelling. Environ Ecol Stat 18:471–493

Pradhan B, Buchroithner MF (2010) Comparison and validation of landslide susceptibility maps using an artificial neural network model for three test areas in Malaysia. Environ Eng Geosci 16(2):107–126

Pradhan B, Lee S (2010a) Landslide susceptibility assessment and factor effect analysis: backpropagation artificial neural networks and their comparison with frequency ratio and bivariate logistic regression modelling. Environ Model Softw 25:747–759

Pradhan B, Lee S (2010b) Regional landslide susceptibility analysis using back- propagation neural network model at Cameron Highland, Malaysia. Landslides 7(1):13–30

Pradhan B, Lee S (2010c) Delineation of landslide hazard areas on Penang Island, Malaysia, by using frequency ratio,

logistic regression, and artificial neural network models. Environ Earth Sci 60(5):1037–1054

Pradhan B, Pirasteh P (2010) Comparison between prediction capabilities of neural network and fuzzy logic techniques for landslide susceptibility mapping. Disaster Adv 3(3):26–34

Pradhan B, Youssef AM (2010) Manifestation of remote sensing data and GIS on landslide hazard analysis using spatial-based statistical models. Arab J Geosci 3(3):319–326

Pradhan B, Lee S, Buchroithner MF (2009) Use of geospatial data and fuzzy algebraic operators to landslide hazard mapping. Appl Geomat 1:3–15

Pradhan B, Lee S, Buchroithner MF (2010a) A GISbased back-propagation neural network model and its cross-application and validation for landslide susceptibility analyses. Comput Environ Urban Syst 34:216–235

Pradhan B, Lee S, Buchroithner MF (2010b) Remote sensing and GIS-based landslide susceptibility analysis and its cross-validation in three test areas using a frequency ratio model. Photogramm Fernerkund Geoinf 1(1):17–32

Regmi NR, Giardino JR, Vitek JD (2010) Modeling susceptibility to landslides using the weight of evidence approach: western Colorado, USA. Geomorphology 115:172–187

Riad PH, Billib MH, Hassan AA, Omar MA (2011) Overlay weighted model and fuzzy logic to determine the best locations for artificial recharge of groundwater in a semi-arid area in Egypt. Nile Basin Water Sci Eng J 4(1):11

Rossi M, Apuani T, Felletti F (2009) A comparison between univariate probabilistic and multivariate (logistic regression) methods for landslide susceptibility analysis: the example of the Febbraro valley (Northern Alps, Italy). Geophys Res Abstr, Vol 11, EGU2009-8399, 2009 EGU General Assembly 2009. https://meetingorganizer.copernicus.org/EGU2009/EGU2009-8399.pdf

Rumelhart DE, Hinton GE, Williams RJ (1986) Learning representations by back-propagating errors. Nature 323:533–536

Saaty TL (1980) The analytic hierarchy process: planning, priority setting, resource allocation. McGraw-Hill, New York, p 287

Saaty TL (1990) An exposition of the AHP in reply to the paper 'remarks on the analytic hierarchy process'. Manage Sci 36:259–268

Saaty TL (1994) Fundamentals of decision making and priority theory with the AHP. RWS Publications, Pittsburgh

Saaty TL, Vargas LG (2001) Models, methods, concepts, and applications of the analytic hierarchy process, 1st edn. Kluwer Academic, Boston, p 333p

Saha AK, Gupta RP, Arora MK (2002) GIS-based landslide hazard zonation in the Bhagirathi (Ganga) valley, Himalayas. Int J Remote Sens 23(2):357–369

Saraswathi K, Senthil R (2017) A comparative study of defuzzification methods for an interacting and non interacting system. Int J Eng Technol Sci Res 4(5):2017

Sarkar S, Kanungo DP (2004) An intergraded approach for landslide susceptibility mapping using remote sensing and GIS. Photogr Eng Remote Sens 70(5):617–625

Schernthanner H (2007) Fuzzy logic method for landslide susceptibility mapping, Rio Blanco, Nicaragua. http://www.geocomputation.org/2007/7A-Evolutionary_Computing_and_Fuzzy_Modelling/7A3.pdf

Suzen ML, Doyuran V (2003) A comparison of the GIS based landslide susceptibility assessment methods: multivariate versus bivariate. Environ Geol 45:665–679. https://doi.org/10.1007/s00254-003-0917-8

Suzen ML, Doyuran V (2004) Data driven bivariate landslide susceptibility assessment using geographical information systems: a method and application to Asarsuyu catchment, Turkey. Eng Geol 71(3–4):303–321

Swingler K (1996) Applying neural networks: a practical guide. Academic Press, London

Tangestani HM (2004) Landslide susceptibility mapping using the fuzzy gamma approach in a GIS, Kakan catchment area, southwest Iran. Aust J Earth Sci 51(3):439–450

Tarboton D (2003) Terrain analysis using digital elevation models in hydrology. In: 23rd ESRI international users conference, July 7–11, 2003, San Diego, California, http://hydrology.usu.edu/dtarb/ESRI_paper_6_03.pdf

Teimouri M, Graee P (2012) Evaluation of AHP and frequency ratio methods in landslide hazard zoning (case study: Bojnord Urban Watershed, Iran). Int Res J Appl Basic Sci 3(9):1978–1984

Turan A (1990) Toroslar'da Hadim (Konya) ve Güneybatısının Jeolojisi, Stratigrafisi ve Tektonik Gelişimi, Doktora Tezi. Selçuk Üniversitesi Fen Bilimleri Enstitüsü, Konya

Turrini MC, Visintainer P (1998) Proposal of a method to define areas of landslide hazard and application to an area of the Dolomites, Italy. Eng Geol 50:255–265

Uromeihy A, Mahdavifar MR (2000) Landslide hazard zonation of the Khorshrostam area, Iran. Bull Eng Geol Environ 58(3):207–213

Vahidnia MH, Alesheikh AA, Alimohammadi A, Hosseinali F (2009) Landslide hazard zonation using quantitative methods in GIS. Int J Civil Eng 7(3):176

Van Den Eeckhaut M, Marre A, Poesen J (2010) Comparison of two landslide susceptibility assessments in the Champagne-Ardenne region (France). Geomorphology 115:141–155

Van Westen CJ, Bonilla JBA (1990) Mountain hazard analysis using PC-based GIS. In: 6th IAEG congress, vol 1. Balkema, Rotterdam, pp 265–271

Van Westen CJ, Rengers N, Soeters R (2003) Use of geomorphological information in indirect landslide assessment. Nat Hazards 30:399–419

Van Westen CJ, Castellanos Abella EA, Sekhar LK (2008) Spatial data for landslide susceptibility, hazards and vulnerability assessment: an overview. Eng Geol 102(3–4):112–131

Vijith H, Madhu G (2008) Estimating potential landslide sites of an upland sub-watershed in Western Ghat's of Kerala (India) through frequency ratio and GIS. Environ Geol 55:1397–1405

Voogd JH (1982) Multicriteria evaluation for urban and regional planning. Delftsche Uitgevers Maatschappij, London, p 367. https://doi.org/10.6100/IR102252

Wilson JP, Gallant JG (2000) Terrain analysis principles and applications. Wiley, New York, p 479p

Yagi H (2003) Development of assessment method for landslide hazardness by AHP. In: Abstract volume of the 42nd annual meeting of the japan landslide society, pp 209–212

Yalcin A (2008) GIS-based landslide susceptibility mapping using analytical hierarchy process and bivariate statistics in

Ardesen (Turkey): comparisons of results and confirmations. CATENA 72:1–12

Yalcin A, Reis S, Aydinoglu AC, Yomralioglu T (2011) A GIS-based comparative study of frequency ratio, analytical hierarchy process, bivariate statistics and logistics regression methods for landslide susceptibility mapping in Trabzon, NE Turkey. CATENA 85:274–287

Yesilnacar E, Topal T (2005) Landslide susceptibility mapping: A comparison of logistic regression and neural networks methods in a medium scale study, Hendek region (Turkey). Eng Geol 79:251–266

Yilmaz I (2009) Landslide susceptibility mapping using frequency ratio, logistic regression, artificial neural Networks and their comparison: a case study from Kat landslides (Tokat—Turkey). Comput Geosci 35:1125–1138

Yilmaz I (2010) Comparison of landslide susceptibility mapping methodologies for Koyulhisar, Turkey: conditional probability, logistic regression, artificial neural networks, and support vector machine. Environ Earth Sci 61(4):821–836

Youssef AM, Pradhan B, Gaber AFD, Buchroithner MF (2009) Geomorphological hazard analysis along the Egyptian Red Sea Coast between Safaga and Quseir. Nat Hazard Earth Syst 9:751–766

Zhou CH, Lee CF, Li J, Xu ZW (2002) On the spatial relationship between landslides and causative factors on Lantau Island, Hong Kong. Geomorphology 43:197–207

Zhu C, Wang X (2009) Landslide susceptibility mapping: a comparison of information and weights-of-evidence methods in three Gorges Area. In: 2009 International conference on environmental science and information application technology, Wuhan, 2009, pp 342–346

Zimmerman H-J (1996) Fuzzy set theory and its applications. Kluwer Academic Publishers, London